Designing a Dy_2 SMM with two well differentiated relaxation processes by using a non-symmetric bis-bidentate bipyrimidine-N-oxide ligand: Comparison with mononuclear counterparts

Ismael F. Díaz-Ortega,†Juan Manuel Herrera,*,†Daniel Aravena,¥ Eliseo Ruiz,¶Tulika Gupta,# Gopalan Rajaraman,*,#H. Nojiri,*,‡Enrique Colacio*,†

† *Departamento de Química Inorgánica, Facultad de Ciencias, Universidad de Granada, Avda. Fuentenueva s/n, 18071, Granada, Spain.*

¥ *Departamento de Química de los Materiales, Facultad de Química y Biología, Universidad de Santiago de Chile (USACH), Casilla 40, Correo 33, Santiago, Chile*

¶*Departament de Química Inorgànica and Institut de Recerca de Química Teòrica i Computacional, Universitat de Barcelona, Diagonal 645, 08028, Barcelona, Spain.*

#*Department of Chemistry, Indian Institute of Technology Bombay, Powai, Mumbai 400076, India.*

‡*Institute for Materials Research, Tohoku University, Katahira, Sendai, 980-8577, Japan*.

ABSTRACT

Herein we report a dinuclear [(μ-mbpymNO){$(tmh)_3Dy$}$_2$] (**1**) single-molecule magnet (SMM) showing two non-equivalent Dy(III) centres, which was rationally prepared from the reaction of $Dy(tmh)_3$ moieties (tmh = 2,2,6,6-tetramethyl-3,5-heptanedionate) and the asymmetric bis-bidentate bridging ligand 4-methyl-bipyrimidine (mbpymNO). Depending on whether the Dy(III) ions coordinate to the N^O or N^N bidentate donor sets, the Dy(III) sites present a NO_7(D_{2d} geometry) or a N_2O_6(D_{4d}) coordination sphere. In consequence, two different thermally activated magnetic relaxation processes are observed with anisotropy barriers of 47.8 K and 54.7 K. *Ab initio* calculations confirm the existence of two different relaxation phenomena and allow to assign the 47.8 K and

54.7 K energy barriers to the Dy(N_2O_6) and Dy(NO_7) sites respectively. Two mononuclear complexes [Dy(tta)$_3$(mbpymNO)] (**2**) and [Dy(tmh)$_3$(phenNO)] (**3**) have also been prepared for comparative purposes. In both cases, the Dy(III) centre shows a NO_7 coordination sphere and SMM behavior is observed with U_{eff} values of 71.5 K (**2**) and 120.7 K(**3**). In all three cases, *ab initio* calculations indicate that relaxation of the magnetization takes place mainly *via* the first excited Kramer state through Orbach, Raman and thermally assisted quantum tunnelling mechanisms. Pulse magnetization measurements reveal that the dinuclear and the mononuclear complexes exhibit hysteresis loops with double and single step structure, respectively, thus supporting their SMM behaviour.

INTRODUCTION

In the last few decades a huge amounts of research efforts have been dedicated to the study of Single Molecule Magnets (SMMs), which are molecular complexes that display slow relaxation of the magnetization and magnetic hysteresis at low temperature[1].SMMs are of current interest not only due to their intriguing physical properties, such as, freezing of the magnetization below the so called blocking temperature (T_B), quantum tunnelling of the magnetization (QTM) and quantum phase interference,[1a] but also due to their potential applications in fields such as molecular spintronics,[2]ultra-high density magnetic information storage,[3] magneto-optics [4]and as qubits for quantum computing at molecular level.[5]SMM behaviour arises from the existence of an energy barrier (*U*) that prevents magnetization reversal when the polarizing field is removed. In principle, the larger the energy barrier height is, the greater T_B should be. However, QTM across the barrier can reduce T_B to an extremely small value even though *U* is very large.[1]

The research activity in the field of SMMs has been mainly focused along four lines: (i) Synthesis of novel members of this family (ii) Study of the structural and electronic factors governing the SMMs behaviour. In this regard, the feedback between experiment and theory has been crucial for the successful development of this line of research. (iii) Deliberate design of SMMs with increasing T_B (temperature at which the magnetic hysteresis opens at zero fieldfor a definite sweep rate) by making use of suitable strategies based on the new generated knowledge (iv) incorporation of SMMs in nanosized-devices. Progress made in research lines (i)-(iii) has allowed the preparation of SMMs with *U*and T_B values as high as 1837 K and 60 K, respectively.[6]This achievements have been mainly reached with high axially symmetric Dy^{III} complexes, because (i) Dy^{III} is a Kramers ion with a doubly degenerate $\pm m_j$ground state, for which QTM should be forbidden in the absence of magnetic field (QTM usually prevents the observation of magnetic hysteresis at zero magnetic field in lanthanide complexes)[1b] (ii) It has a large magnetic moment in the ground state and (iii) the anisotropic oblate-shaped *f* electron density of the Dy^{III} ion requires an appropriate axial crystal field to induce axial magnetic anisotropy in the ground state.[1b] The large is the axial magnetic anisotropy (complex with ideal axial symmetry and shorter Dy^{III}-donor bond distances involving axial positions), the smaller QTM and larger T_B.

The slow relaxation of the magnetization passing from a magnet state to a paramagnetic state in Dy^{III} SMMs is a very intricate process, which can takes place through the ground and/or the first and/or even higher low lying excited states, generally via multiple processes (QTM, one-phonon direct, two-phonon Raman and Orbach).[1] It is worth noting that for some SMMs two thermally activated processes of molecular origin have been observed, even in mononuclear and polynuclear complexes with crystallographically equivalent Dy^{III} ions.[7] Moreover, in a few cases, it has been demonstrated by magnetic

dilution studies that one of these processes is really intermolecular in origin.[8]Regardless of the origin of the relaxation processes (molecular with equivalent or non-equivalent Dy^{III} ions or intermolecular), their presence was generally a matter of serendipity, as the ligand was not deliberately designed to afford two non-equivalent Dy^{III} sites. In view of this we have decided to design a new neutral bis-bidentate bridging ligand, 4-methyl-bipyrimidine-2-N-oxide (mbpymNO) with two different bidentate donor sets and chelating rings (six-membered NO and five-membered N2), which, when acts in a bis-bidentate coordination mode, will mandatorily afford Dy^{III} complexes with two different Dy^{III} coordination spheres. Although over the last few years pyridine N-oxide derivatives have been used as ligands for preparing Dy^{III} containing SMMs, the number of reported examples is still limited.[9] The present paper reports the synthesis, crystal structure, detailed ac and dc magnetic studies and ab initio theoretical calculations of the dinuclear complex [(μ-mbpymNO){$(tmh)_3Dy$}$_2$] (**1**) as well as of the mononuclear complexes [$Dy(tta)_3$(mbpymNO)] (**2**) and [$Dy(tmh)_3$(phenNO)] **(3)** for comparative purposes. Based on previous results with diazine and tetrazine complexes containing β-diketonato ancillary ligands[10] the reported complexes are expected to exhibit SMM behaviour. The aim of this study is threefold (i) to confirm the existence of two well differentiated thermally activated processes, (ii) to prove the single-ion origin of these relaxation processes, (iii) to assign each relaxation processes to each type of Dy^{III} coordination sphere and (iv) to draw useful conclusions for future development of the field.

EXPERIMENTAL SECTION

General procedures

1,10-Phenanthroline 1-oxide (phenNO) was prepared according to the reported procedure described by Corey et al. [11]The ligands 2,2,6,6-tetramethyl-3,5-heptanedione (Htmh), 2-

Thenoyltrifluoroacetone (Htta), solvents and dysprosium salts were purchased from commercial sources and used as received.

Synthesis of ligand 4-methyl-2,2'-bipyrimidine-2-oxide (mbpymNO). This ligand was prepared in two steps. First, 2-cyanopyrimidine (0.02 mol, 2.1 g), hydroxylamine hidrochloride (0.04 mol, 2.8 g) and sodium hydrogen carbonate (0.04 mol, 3.36 g) were dissolved in water (40 mL) and stirred vigorously at room temperature. After one hour, a white precipitate corresponding to the intermediate product (E)-*N'*-hydroxypyrimidine-2-carboximidamide appeared.[12] The solid was filtered, washed with water, dried under vacuum and used in the next step without any further purification. In a second step, 0.018 mol of (E)-*N'*-hydroxypyrimidine-2-carboximidamide were mixed with the equimolar amounts of 3-Ethoxy-2-methylpropenal and trifluoroacetic acid in 25 mL of 2-propanol and the resulting solution was heated at 80 ºC for 12 h. After this time, the resultant mbpymNO ligand precipitated as a white powder which was filtered, washed with ethanol and dried under vacuum. Yield: 76 %. Anal.Calcd. (found) for $C_9H_8N_4O$: C, 57.42 (55.05); H, 4.28 (4.54); N, 29.78 (30.50). ^{1}H NMR (400 MHz, DMSO-d_6): δ (ppm) = 8.99 (d, *J = 4.96 Hz*, 2H), 8.69 (s, 1H), 8.29 (s, 1H), 7.66 (t, *J = 4.92 Hz*, 1H), 2.33 (s, 3H). MS (ESI): *m/z*calcd. (found) for $C_9H_9N_4O^+$: 189.08 (189.0777).

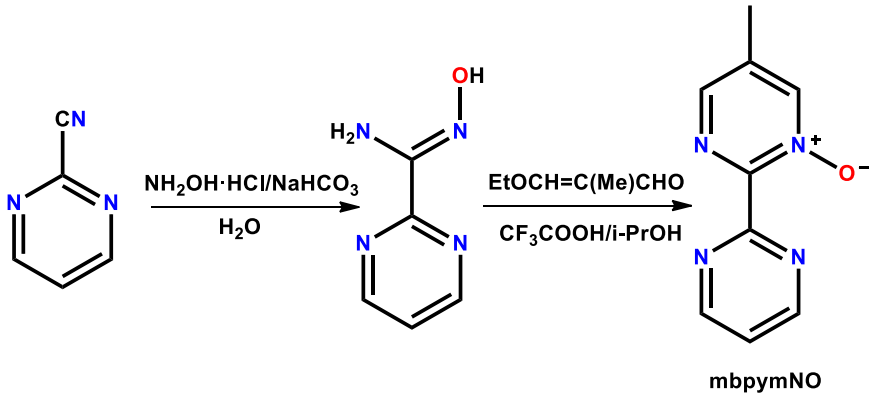

Scheme 1.- Synthesis of the mbpymNO ligand.

Synthesis of complexes

[{Dy(tmh)$_3$}$_2$(μ_2-mbpymNO)]·MeOH (1).0.375 mmol of Dy(NO$_3$)$_3$·6H$_2$O dissolved in methanol (5 mL) were added to a solution of Htmh (1.125 mmol) and Et$_3$N (1.125 mmol) in methanol (5 mL). The solution was stirred for 10 min. and then added dropwise to a solution of 4-methyl-2,2'-bipyrimidine-2-oxide (mbpymNO) (0.187 mmol) dissolved in 5 mL of methanol. The resulting solution was allowed to stand at room temperature. Partial evaporation of the solvent afforded a good crop of **1** as single crystals which were filtered, washed with a minimum amount of ethanol and air dried. Yield *ca.* 50 %. Anal.calc. for C$_{75}$H$_{122}$N$_4$O$_{13}$Dy$_2$·CH$_3$OH: C, 55.49; H, 7.72; N, 3.41. Found: C, 56.20; H, 7.80; N, 3.21.

[Dy(tta)$_3$(mbpymNO)] (2). This complex was prepared as **1** but using Htta instead ofHtmhand a molar ratio [Dy(tmh)$_3$]:mbpymNOof 1:1.Yield *ca.* 50 %. Anal.calc. for C$_{33}$H$_{20}$N$_4$O$_7$F$_9$S$_3$Dy (**1**): C, 39.10; H, 1.99; N, 5.52. Found: C, 40.03; H, 2.23; N, 5.30.

[Dy(tmh)$_3$(phenNO)] (3). This complex was prepared as **2** but using the ligand Htmh instead of Htta and 1,10-phenanthroline-N-oxide (phenNO) instead of mbpymoNO. Yield *ca.* 65 %. Anal.calc. for C$_{45}$H$_{65}$N$_2$O$_7$Dy (**3**): C, 59.49; H, 7.21; N, 3.1. Found: C, 58.67; H, 7.68; N, 3.32.

X-ray Crystallography

Suitable crystals of complexes **1 - 3** were mounted on a Bruker D8 Venture (Mo Kα radiation, λ = 0.71073 Å, Photon 100 CMOS detector). Details of the crystals, data collection and refinement parameters are reported in Supporting Information (Table S1). Once the data were processed (raw data integration, merging of equivalent reflections and empirical correction of the absorption), the structures were solved by either Patterson or Direct methods and refined by full-matrix least-squares on weighted F$_2$ values using the SHELX suite of programs[13] integrated in Olex2.[14] Selected bond lengths and angles can also be found in Supporting Information (Tables S2-S4).

Physical measurements

Elemental analyses were carried out at the "Centro de Instrumentación Científica" of the University of Granada on a Fisons-Carlo Erba analyser model EA 1108. FT-IR spectra were recorded with a Bruker Tensor 27 spectrometer using an ATR accessory. Direct (dc) and alternating (ac) current susceptibility measurements were performed with a Quantum Design SQUID MPMS XL-5 device. Ac experiments were performed using an oscillating *ac* field of 3.5 Oe and frequencies ranging from 1 to 1500 Hz. Ac magnetic susceptibility measurements in the range 1 – 10000 Hz were carried out with a Quantum Design Physical Property Measurement System using an oscillating *ac* field of 5 Oe. Low-temperature magnetization measurements were performed by means of a conventional inductive probe in pulsed-magnetic fields. The temperature was reached as low as 0.4 K using a ^{3}He cryostat.[15] Polycrystalline specimens were mounted in a capillary tube made of polyimide. Samples of approximately 20 mg were not fixed within the sample tube and then they aligned along the magnetic field direction. Subsequently, a magnetic field was applied several times until orientation effect was saturated and the magnetization curves obtained in further shots were found to be identical.

Computational Methodology

MOLCAS 8.0 program package[16] has been used to perform post-Hartree-Fock *ab initio* calculations. Using multiconfigurational approach relativistic effects were treated in two steps, based on Douglas-Kroll Hamiltonian. For the generation of basis sets scalar terms were included which has been used to determine spin-free wave functions and also energies through the use of the complete active space self-consistent field(CASSCF) method.[17] Thus, spin-orbit free states were obtained by employing the RASSCF method whereas spin-orbit coupling has been taken into account using RASSI-SO method[18] which uses CASSCF wave functions as the basis sets and multiconfigurational wave

functions as input states. The resulting wave functions and the energies of the molecular multiplets were used for the calculation of the magnetic properties and g tensors of the lowest state using a specially designed routine SINGLE_ANISO.[19] As a consequence, the magnetic properties of a single magnetic ion are calculated by a fully *ab initio* approach in which the spin-orbit coupling is considered non-perturbatively. The active space in the CASSCF calculations comprised 9 electrons in 7 orbitals for Dy^{III} ion, with a [ANO-RCC... 9s8p6d4f3g2h.] basis set for Dy^{III}, [ANO-RCC...4s3p1d.] for N and O, [ANO-RCC...4s3p1d] for S, [ANO-RCC...3s2p.] for C and F, [ANO-RCC...2s.] for H. 21 sextets, 224 quadruplets and 158 triplets were computed, while in RASSI, we have mixed 21 sextets, 128 quadruplets and 98 doublets. For complex **1**, an additional approach was considered (approach II) with: Basis sets [ANO-RCC...7s6p4d2f.] for Dy^{III}, [ANO-RCC...3s2p.] for N and O, [ANO-RCC...4s3p] for S, [ANO-RCC...3s2p.] for C and F, [ANO-RCC...2s.] for H. Calculations with approach II were executed at the ground state (S = 6) with 21 configurations (sextets). All the ANO-RCC basis sets have been adopted from MOLCAS ANO-RCC library.[16b] In order to save disk space, Cholesky decomposition possessing a threshold of $0.2*10^{-7}$ has been incorporated for our calculations.[20] Magnetic exchange interactions, exchange spectrum and all other magnetic properties of Dy_2 dinuclear complex has been deduced within the POLY_ANISO[21] routine based on the *ab initio* results of individual metal fragments.[22]

RESULTS AND DISCUSSION

Syntheses and Crystal Structures. Single crystals of the dinuclear complex **1** appeared after partial evaporation of a methanolic solution containing a mixture of $Dy(NO_3)_3 \cdot 6H_2O$, triethylamine, the β-diketone ligand Htmh and the *N*-oxide ligand mbpymNO in a molar ratio 1:3:3:0.5. The mononuclear complexes **2** and **3** were obtained following a similar procedure from the respective β-diketone (Htta for **2** and Htmh for **3**)

and the N-oxide ligands (mbpymNO for **2** and phenNO for **3**), but in these cases the molar ratio of the reactants was 1:3:3:1 (see Scheme 2). Efforts to prepare the dinuclear [{Dy(tta)$_3$}$_2$(μ_2-mbpymNO)] analogue were unsuccessful and only the mononuclear complex was obtained. Queerly, we have also been unable to isolate the mononuclear [{Dy(tmh)$_3$}$_2$(μ_1-mbpymNO)] complex and all the essays performed lead to the dinuclear specimen, regardless the Dy:mbpym non stoichiometric ratio used in the reaction.

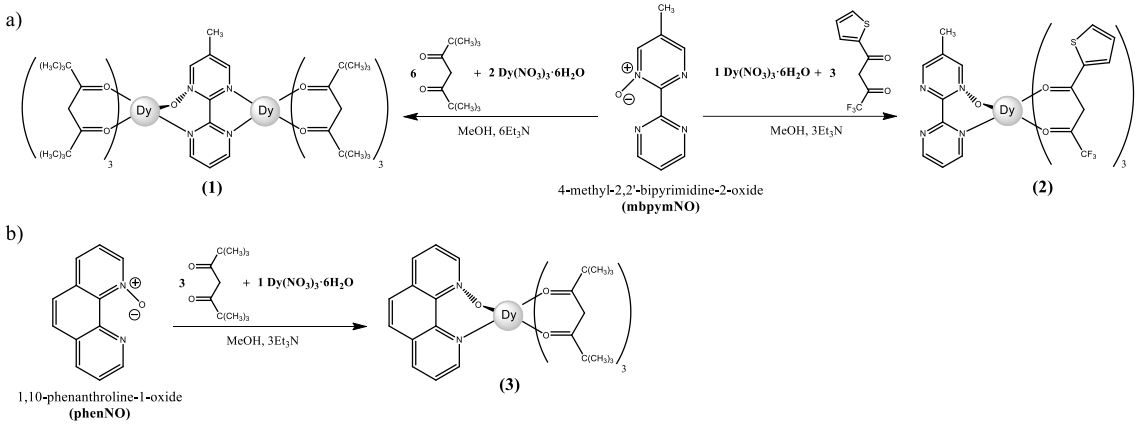

Scheme 2.- Syntheses of complexes **1 – 3**.

The dinuclear complex **1** crystallizes in the monoclinic P2$_1$/c space group and the structure consists of two [Dy(tmh)$_3$] moieties connected through the non-symmetric bis-bidentate mbpymNO ligand. Thus, the Dy^{III} centres show different coordination spheres. Whereas the ion Dy1 is coordinated to the mbpymNO ligand through the N^O bidentate site (NO$_7$ coordination sphere), the Dy2 centre is coordinated to the opposed N^N site (N$_2$O$_6$ coordination sphere).Analysis of the eight-coordinated geometries around the Dy centres by the continuous-shape-measures (CShMs) method[23]reveals that Dy1 and Dy2 show coordination spheres that are intermediate between several ideal geometries, with the lowest CShMs parameters for the D$_{2d}$ triangular dodecahedron (1.161) and D$_{4d}$square antiprism (0.805), respectively (Table S5). The Dy-O$_{tmh}$ bond distances in both centres fall between 2.2754 Å (Dy1-O2) and 2.3556 Å (Dy1-O6), as expected for this kind of

complexes. The Dy1-$O_{mbpymNO}$ bond distance is also similar (2.3725 Å), and much shorter than Dy-$N_{mbpymNO}$ distances which are found in the range between 2.6080 Å and 2.6462 Å. The average Dy-O distance in Dy2 atom are slightly shorter than that in Dy1 (2.30 Å and 2.32 Å, respectively). The pyrimidine rings in the mbpymNO ligand are mutually twisted an angle of 17.33º(figure S1) and the Dy1-O1-N1 angle deviates significantly from linearity with a value of 127.23(3)º. Within the molecule, the Dy1-Dy2 distance through the mbpymNO ligand is 7.099 Å. The shortest intermolecular distance between Dy centres is 12.454 Å.

Regarding the mononuclear complexes, **2** and **3**, they crystallize in spaces group *Pbcn* (orthorhombic) and *P-1* (triclinic) respectively. For **2**, the structure consists of mononuclear [$Dy(tta)_3$(mbpymNO)] entities where the Dy_{III} center exhibits a NO_7 coordination spherewith one nitrogen and one oxygen atoms belonging to the mbpymNO ligand and the six others oxygen atoms to three deprotonated tta ligands. The Dy-O_{tta}bond distances are in the range 2.303(4) – 2.361(3) Å, quite similar to the Dy-$O_{mbpymNO}$ distance of 2.317(4) Å and significantly shorter than the Dy-$N_{mbpymNO}$ bond distances of about 2.6 Å (selected bond distances and angles are reported in table S3). For **3**, despite the replacement of ligands mbpymNO and tta by phenNO and tmh respectively, the structure is quite similar to **2**. The NO_7coordination environment around the Dy_{III} centre shows Dy-O and Dy-N bond distances which are in the same range than those observed for**2** (Table S4). Analysis of the coordination spheres around the Dy centres by the CShMs method (Table S5) reveals that in both cases the geometry is close to a square-antiprismatic polyhedron (SAPR). Nevertheless, for**2** the CShMs deviation parameter from an ideal SAPR (0.791) is slightly higher than that shown by **3** (0.566). It should be noted that the mononuclear complexes [$Dy(tta)_3$(phen)] (phen = 1,10-phenanthroline) and [$Dy(tta)_3$(bipy)] (bipy = 2,2'-bipyridine) show almost identical CShMs values between

them (0.546 and 0.555) and with compound **3**, despite the different bidentate N,N or N,O and β-diketonate ligands.[24] In spite of thesmall bite of the bidentate N-oxide ligand [angle O(1)-Dy(1)-N(4) = 67.60(13)º (**2**); angle O(1)-Dy(1)-N(2) = 65.06(12) (**3**)] compared to those exhibited by the β-diketonate ligands [in the range between 72.22(12)º for O(6)-Dy(1)-O(7) – 73.12(13) for O(2)-Dy(1)-O(3) for **2** and 71.67(10) for O2-Dy1-O3 – 73.27(9) O4-Dy1-O5 for **3**] the NO_7 coordination spheres are not seriously distorted fromSAPR. The structural features involving the n-oxide ligands mbpymNO (**2**) and phenNO (**3**) are significantly different in both cases, due to the intrinsic nature of each ligand. In the mbpymNO ligand, the two pyrimidine moieties can rotate freely through the C5-C6 bond, whereas for the phenNO ligand an equivalent rotation of the pyridine rings through the C11-C12 bond is not possible. Thus, in **2** the pyrimidine rings of the mbpymNO ligand are twisted by 48.45ºrelative to each other (Figure S1a). In**1**, the simultaneous coordination of the ligand to two Dy_{III} centres forces the pyrimidine rings to adopt a conformation more planar than in **2**. The Dy1-O1-N1 angle deviates strongly from linearity with a value of 122.0(3)º. For **3**, the phenNO ligand is slightly bent, with the dihedral angle between the planes containing the aromatic rings N2-C10-C9-C8-C7-C11 and C12-C4-C3-C2-C1-N1 only 11.17º (Figure S1b and Table S4). The N1-O1-Dy1 angle also deviates strongly form linearity [130.6(4)º] although to a less extent than in the cases of **1** and **2**.

The shortest intermolecular Dy-Dy distances are 9.084 Å for **2** and 9.309Å for **3** and although in both cases, weak π-π interactions exist between the aromatic rings of adjacent molecules (Figures S2 and S3), the Dy_{III} centres can be considered as isolated from a magnetic point of view.

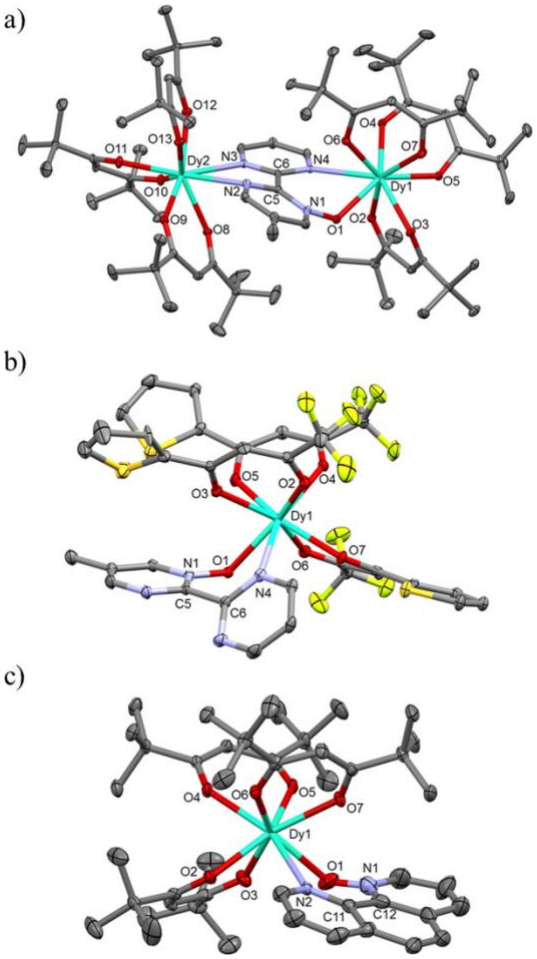

Figure 1.- Crystal structures of complexes **1** (a), **2** (b) and **3** (c). Lattice solvents as well as hydrogen and disordered atoms have been omitted for the sake of clarity. Ellipsoids are drawn at 50 % probability.

Magnetic properties. The thermal variation of the dc magnetic data ($\chi_M T$ vs. T plots) for complexes **1 – 3** (Figure S4) shows $\chi_M T$ values at T = 300 K of27.59 $cm^3 \cdot K \cdot mol^{-1}$ (**1**), 13.68 $cm^3 \cdot K \cdot mol^{-1}$ (**2**), 14.66 $cm^3 \cdot K \cdot mol^{-1}$ (**3**), which are close to the theoretical value of 14.17 $cm^3 \cdot K \cdot mol^{-1}$ per Dy^{III} ion in the free-ion approximation ($4f^9$, J = 15/2, S = 5/2, L = 5, g = 4/3, $^6H_{15/2}$). Upon cooling, the $\chi_M T$ productsdecrease continuously down to reach values of21.04 cm^3 K mol^{-1} (**1**), 11.96 cm^3 K mol^{-1}(**2**) and12.99 cm^3 K mol^{-1} (**3**) at 2 K. For the mononuclear complexes **2** and **3**, this behaviour is due to the combined effects of the thermal depopulation of the M_J sublevels of the $^6H_{15/2}$ ground term split by crystal

field effects and possible intermolecular dipolar interactions. For the dinuclear complex **1**, additional weak intramolecular antiferromagnetic exchange interactions between the Dy^{III} centres through the mbpymNO bridge-ligand could be responsible for the sharp decrease in $\chi_M T$ at very low temperature. The *M vs H* plots at 2 K for complexes **1 – 3** show a rapid increase of the magnetization below 1 T and then a very slow linear increase to reach values of9.88 $N\mu_B$ (**1**)(4.94 $N\mu_B$ per Dy^{III} ion), 5.89 $N\mu_B$ (**2**) and 5.94 $N\mu_B$ (**3**) at 5 T. These values are much lower than the expected saturation value of 10 $N\mu_B$ per Dy^{III} ion ($M_S/N\mu_B = g_J J = 10\ N\mu_B$) and are compatible with the existence of strong crystal-field effects leading to approximate axial symmetry with far-separated energy levels and, therefore, with a well isolated ±15/2 ground state.[6d]

Single Molecule Magnet (SMM) behaviour.

As expected from the easy-axis anisotropy of the Dy^{III} ion (see below for *ab initio* calculations), complexes **1**-**3** show frequency and temperature dependence of the out-of-phase magnetic susceptibility (χ'_M) at zero field, which is indicative of slow relaxation of the magnetization and SMM behaviour. For compound **1**, the temperature dependence of the χ'' plot shows a broad signal devoid of any neat maximum between 7- 20 K, a clearly visible shoulder between 4 K (150 Hz) and 5 K (1400 Hz) and a relatively strong increase of χ''_M below 3 K (Figure S5). This behaviour can be due to overlapping of different relaxation processes, including fast QTM relaxation, which is responsible of the strong increase of χ''_M at very low temperature. The QTM relaxation process dominates in intensity and consequently modulates the relative intensity of the other signals.

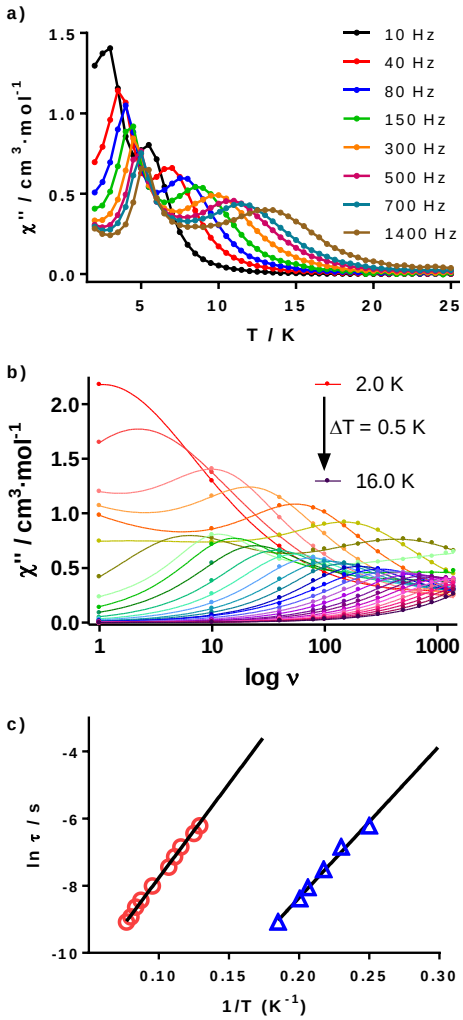

Figure 2.-Temperature dependence (top) and frequency dependence (middle) of out-of-phase ac susceptibility signals at 1000 Oe (top) for complex **1**. Solid lines are only a guide for the eye. Arrhenius plots for the slow (red circles) and fast (blue triangles) relaxation processes for complex **1**.

In order to eliminate entirely or partially the quantum tunnelling relaxation of the magnetization (QTM), ac measurements were carried out in the presence of a small external *dc* field. To know the optimal magnetic field that induces a larger relaxation time, the frequenc y dependence of the *ac* out-of-phase signal at 3 K at different fields was analyzed to extract the relaxation times at each magnetic field. The field dependence of the relaxation times (Figure S6) clearly shows that τ increases until 1000 Oe and then remain almost constant. Therefore, *ac* measurements were carried out in the presence of

an external *dc* field of 1000 Oe. Under these conditions, two maxima were observed in the 3.0 K (10 Hz) - 5.5 K (1400 Hz) and 5.5 K (10 Hz) - 13.5 K (1400 Hz) ranges, and the low temperature tail due to QTM almost disappears (see Figures 2a and S7). The presence of two relaxation processes SR (at high temperature) and FR (at low temperature) could be due to the existence of two different Dy_{III} centres in the structure. The fit of the Cole-Cole plot (Figure S8) to the Debye model with the CCFIT program[25]afforded the temperature dependence of the relaxation times for the SR and FR relaxation processes. The fit of these data to the Arrhenius law (see Figure 2c) led the following parameters U_{eff} = 54.7 K and τ_o = 1.7(3) x 10^{-6} s and U_{eff} = 47.8 K and τ_o = 1.5(4) x 10^{-8} s, for the SR and FR relaxation processes, respectively.

At zero dc field, the mononuclear complexes **2** and **3** exhibit frequency and temperature dependence of the out-phase susceptibility signal (χ''_M) below 15 K (Figures S9a and S12a respectively), which is indicative of slow relaxation of the magnetization and SMM behaviour. However, the presence of an intense increase of the the χ''_M signals below ~ 7K due to fast QTM precludes in both cases the observation of neat maxima.

When a 0.1 T external *dc* magnetic field was applied to cancel or reduce QTM (this is the optimal field for both compounds inducing a larger relaxation time, see Figure S11), well defined χ''_M signals appeared in both cases (Figures S9b and S12b respectively). For**2,**the χ''_M maxima appear between 4.6 K (60 Hz) and 10.2 K (10000 Hz).For **3**,those maxima are slightly displaced to higher temperatures [6.25 K (10 Hz) – 11.5 K (1400 Hz)].Fitting of the frequency dependence of χ''_M at different temperatures to the generalized Debye model, afforded the relaxation times of the magnetization (τ) at each temperature (Figure 3).The effective energy barrier for the reversal of the magnetization (U_{eff}) and the pre-exponential factor τ_0 calculated from the fit of τ to an

Arrhenius law were: U_{eff} = 71.5 (5)K and τ_o = 1.9(2) x 10^{-8}s and U_{eff} = 120.7(4) K and τ_o = 3.9(4) x 10^{-9} s, for **2** and **3**, respectively.

The deviation of the data from the Arrhenius law at low temperatures is indicative of the existence of several competing relaxation processes. The Cole-Cole plots for these complexes show semicircular shapes [Figures S10 (**2**) and S13 (**3**)] with α values ranging between 0.164(5.6 K) – 0.202(10.6 K) for **2** and 0.215(7 K) – 0.218(12 K) for **3**, which support the existence of several relaxation processes in both cases. Since in the temperature ranges studied (T > 6 K and 0.1 T) QTM and direct relaxation processes are expected to be almost negligible, we fitted the magnetic data to eq. 1, which considers that Raman and Orbach processes contribute simultaneously to the relaxation of the magnetization.

$$\tau^{-1} = BT^n + \tau_{0}^{-1} exp(-U_{eff} /k_B T) \quad \text{(Eq. 1)}$$

The extracted parameters were: B = 0.24, n = 4.9, U_{eff} = 99.6 K and τ_o = 2.1 x 10^{-9} s for **2** and B = 0.005, n = 5.2, U_{eff} = 159.1 K and τ_o = 1.9 x 10^{-10} s for **3**. U_{eff} are higher than those obtained from the simple Arrhenius law, while the pre-exponential factors τ_0 decrease almost one order of magnitude.

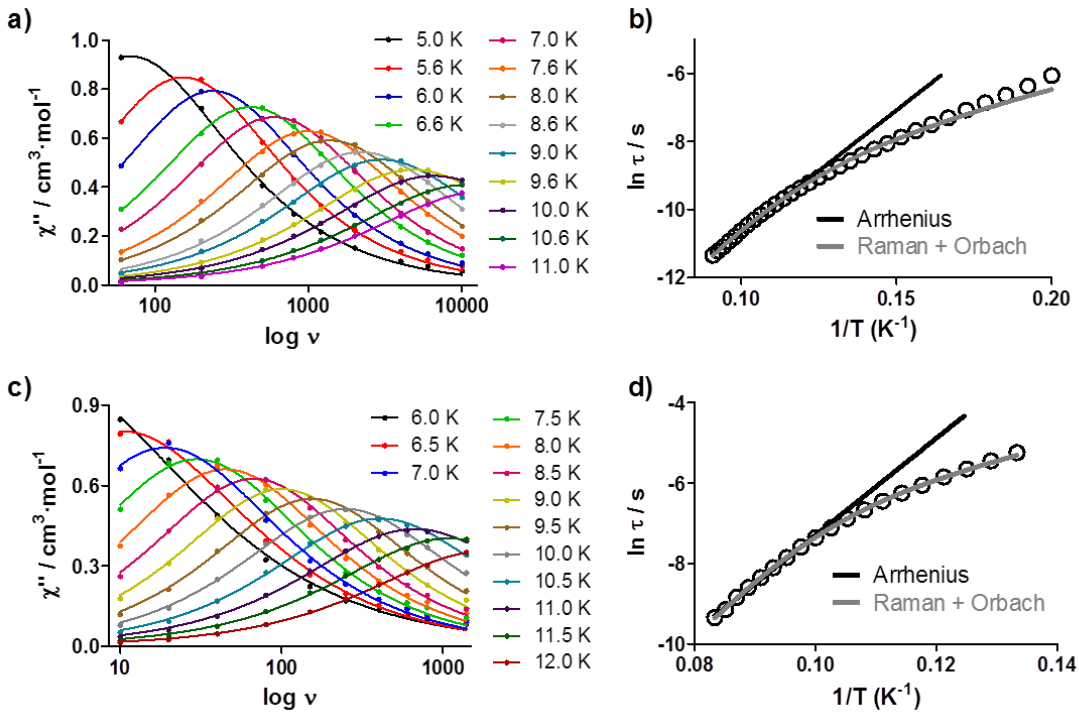

Figure 3.-Frequency dependence of the out-phase susceptibility signal χ"Mof complexes**2** (a) and **3** (c)at different temperatures under an optimized applied dc field of 0.1 T (left). lnτ vs. T^{-1} plot for complexes**2**(b) and **3** (d). The solid lines represent the best fits of the experimental data to the Arrhenius law for a thermally activated process (black line) or to an Orbach-Raman relaxation process (grey line).

Ab initio calculations

In order to confirm the axial anisotropy of the ground state and to gain insight into the mechanism of the slow magnetic relaxation of **1-3**, we have performed electronic calculations on their X-ray structures based on CASSCF+RASSI-SO/SINGLE_ANISOmethod[19] using MOLCAS 8.0 code.[16] The energy spectrum, g-tensors and wavefunctions for the eight Kramers doublets (KDs) arising from the splitting of the ground $^6H_{15/2}$ spin-orbit ground atomic term, which is inducedby the CF in compounds**1-3**, are gathered in Tables 1, 2 and S6-S9.

Table 1. CASSCF+RASSI calculated energies for the eight Kramer's doublets stemming from the ground $^6H_{15/2}$ multiplet for compounds **1, 2** and **3** (method I).

Kramers' doublet (KD)	Energy (cm^{-1})			
	1-Dy1	**1-Dy2**	**2**	**3**
1	0.0	0.0	0.0	0.0
2	109.78	157.20	82.26	140.69
3	144.24	232.53	130.72	200.43
4	202.47	273.49	153.89	230.11
5	256.20	316.34	188.04	261.71
6	281.69	395.47	260.96	337.82
7	443.79	468.42	291.77	368.75
8	571.47	553.03	423.15	483.71

Table 2.-*g*-factors and wavefunction for the ground Kramers' doublet of compounds **1**, **2** and **3** (method I).

Compound	$\mathbf{g_x}$	$\mathbf{g_y}$	$\mathbf{g_z}$	**Wavefunction**
1-Dy1	0.04	0.07	19.68	0.98 |±15/2> + 0.02 |±13/2>
1-Dy2	0.01	0.01	19.52	0.94 |±15/2> + 0.04 |±11/2>
2	0.02	0.03	18.92	0.93|±15/2>+0.07|±3/2>
3	0.00	0.00	19.58	0.96 |±15/2> + 0.03 |±11/2>

For compound **1**, the calculated energy spectrum of the eight KDs span up to 571 $cm^{-1}$and 553 cm^{-1}, with subsequent excited spin-orbit term lying at 3050 and 3066 cm^{-1} for Dy1 and Dy2 sites, respectively. The anisotropy of the ground Kramers doublet state (KD1)for both Dy sites (Dy1 and Dy2) is of pure Ising type as indicate the large magnetic moments with g_z approaching towards ideally pure $m_J=\pm15/2$ state ($g_z=20$)(Tables 2, S6 and S7), which favors the slow relaxation of the magnetization and the SMM behavior.[26] The Ising nature of the ground state is also supported by the corresponding wavefunctions. Thus, the wavefunctions associated to KD1 arealmost pure $|\pm15/2>$ for

both Dy sites whereas those associated to KD2 show a high degree of mixing (Tables 2, S6-S7). Comparatively, associated transverse component is larger for Dy2 site as compared to the Dy1 site for all the KDs including ground state. This clearly implies non-symmetric nature of the two Dy sites within complex **1**. It is worth noting that in both cases, axiality of the excited states decreases till forth KD with proportional increase of magnetic moment along XY plane. From this KD, the axiality increases again graduallyto reach almost pure Ising type in the eighth KD,thus replicating the anisotropy of ground state (KD1) (Tables S6 and S7). This mirror symmetry explicitly represents systems possessing low symmetry around the metal ions. KD1 is found to possess zero magnetic moment in the XY plane and it is entirely oriented along Z axis.

The calculated magnetic moment of the ground state for Dy1 and Dy2 (Figure 4) lies close to the two tmh β-diketonato ligands at opposite sides of each Dy atom, which provide an appropriate axialcrystal field with the remaining positions in the equatorial plane occupied by the oxygen atoms of the other tmh bidentate ligand and the N,N or N,O atoms belonging to the neutral bis(bidentate) mbpymNO ligand. In this disposition, the oblate electron density of the $Dy^{III}$is forced to be located in the equatorial plane, thus diminishing the electrostatic repulsions with the oxygen atoms of the two β-diketonato ligands defining the axial crystal field and the anisotropic axis, as qualitatively predicts the oblate-prolate model.[27] In fact, the deviation of *ab initio* computed ground state g_{zz} orientation with respect to the electrostatic anisotropy axis (Figure S14) is actually very small.

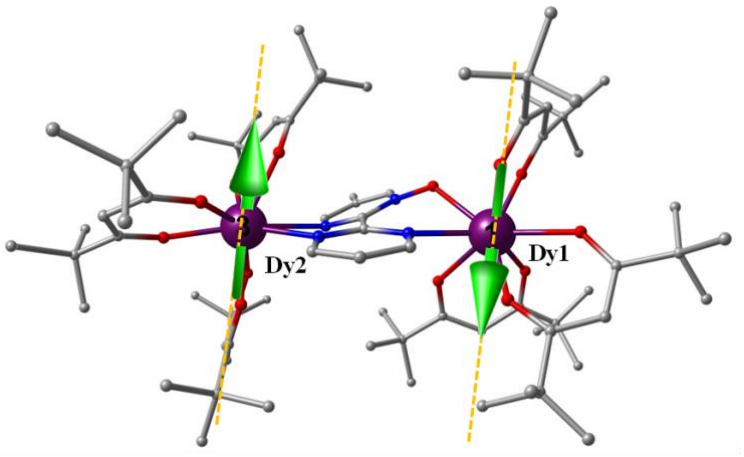

Figure 4.- Crystal structure of complex **1** showing *ab initio* computed principal anisotropy direction (g_{zz}) of both the Dy sites in their ground state Kramers doublets.

It is worth remembering that magnetic relaxation in lanthanides is found to take place fundamentally through the following pathways in the absence of intermolecular interactions:[28,29](i) QTM within the ground state KD1 which arises from its large transverse anisotropy (ii) Orbach/Raman processes which accounts for the relaxation via excited KDs promoted fundamentally by the non-coincidence of the principle anisotropic axes. (iii) Thermally assisted QTM (TA-QTM) via excited KDs states due to their non-Ising nature. The magnitude of these spin-phonon relaxations depend on the square of the transverse magnetic moment. In view of this, and with the aim to reveal the magnetic relaxation pathways of Dy1 and Dy2 in compound **1**, we have calculated the mean absolute values of the transverse magnetic moments between the connecting pairs of opposite magnetization. Qualitative mechanism of relaxation obtained from *ab initio* calculations for **1** and for both the Dy_{III} sites is shown in Figure 5. Here the states are arranged according to the values of their magnetic moments. The number at each arrow connecting any two states is the mean absolute value of the matrix elements of the transition magnetic moments between the corresponding states. Pure Ising nature of ground state anisotropy (g_{zz} value of 19.68, 19.52 respectively for Dy1 and Dy2

sites)induces almost completely suppressed QTM in both Dy^{III}ions in **1**(the matrix element of the transition magnetic moment is 0.02 μ_B(Dy1) and 0.003 μ_B(Dy2),and an efficient spin relaxation mechanism is only expected when the transition magnetic moment is above 0.1 μ_B).[30]

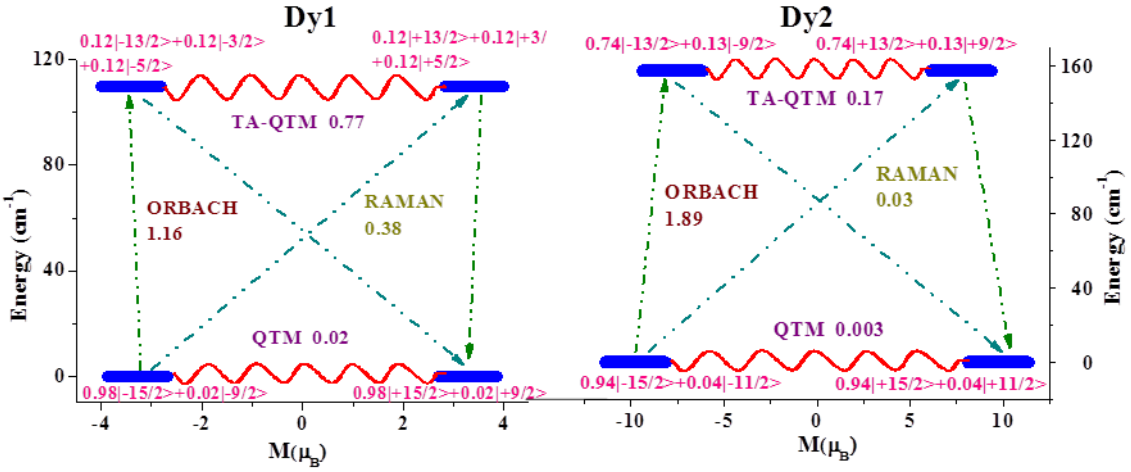

Figure 5.- *Ab initio* computed relaxation mechanism for both the Dy^{III} sites in complex **1**.

For both centres, the first excited KD (KD2) shows considerable transverse anisotropy leading to relaxation via this state. The energy gap between the first and the ground KD (KD2 – KD1) is computed to be 109.8 cm^{-1} and 157.2 cm^{-1} for Dy1 and Dy2 sites respectively. This outlines the existence of two different relaxation phenomena, corroborating the experimental *ac* magnetic measurements. Moreover, substantial misalignment of the first excited g_{zz} axis with respect to that in the ground state, particularly for the Dy1 site (67° for Dy1 and 17.2° for Dy2) reinforces the magnetic relaxation via the first excited state. This is strongly supported by our computed spin-phonon relaxation (Orbach/Raman) contribution from the KD2 as (1.16/0.38) and (1.89/0.03) for Dy1 and Dy2 sites respectively. Relaxation occurrence within this KD2 states are further corroborated by significant tunnelling contribution (TA-QTM as 0.77 $\mu_B$and 0.17 μ_B for Dy1 and Dy2, respectively). In view of the above considerations and taking into account that the blocking barrier is determined by the closest pathways with

larger transition magnetic moments[31] both Orbach and TA-QTM relaxations via the first excited KD2 are operative. However, higher axiality, lower transverse anisotropy as well as smaller matrix elements corresponding to QTM and TA-QTM contribute to comparatively greater barrier value for individual Dy2 centre compared to Dy1. However, the calculated energy gaps for Dy1 and Dy2 that determine the thermal energy barriers are rather higher that those extracted from experimental results, assuming a value of 33 cm^{-1} for Dy1 and 38 cm^{-1} for Dy2, corresponding to the FR and SR relaxation processes, respectively. This deviation between calculated and experimental results is rather usual and could be due, among other factors to (i) the existence of additional relaxation pathways, particularly QTM in the ground state promoted by dipolar and hyperfine interactions, which reduces the expected pure Orbach thermal energy barrier to an effective value (U_{eff}), (ii) limitations inherent to the computational tool and (iii) possible modifications occurring in the structure at very low temperature.

Although calculations indicate negligible QTM, experimental results (Figure S5) show that at zero field QTM is the dominant relaxation process at low temperature, probably due to intermolecular and/or hyperfine interactions which are known to favour this type of relaxation. In order to suppress intermolecular dipolar interactions, we prepared a magnetically diluted analogue of **1** using a Dy/Y =1/10 molar ratio (**1'**). The *ac* measurements on **1'** at zero dc field and 1200 Hz show that the QTM is only partly suppressed as a net maximum and a shoulder are clearly visible at almost the same temperatures as those for **1** measured in the presence of a dc field of 1 kOe. Moreover, an intense tail due to QTM is observed below 5 K. When *ac* measurements on **1'** are performed in the presence of a magnetic field of 1 kOe (Figure S15) both χ''_M peaks for the SR and FR processes do not appreciably shift with respect to their positions in the neat compound **1**at 1kOe. However, the very small tail at very low temperature for **1** at

1kOe due to QTM disappears, as expected from the reduction of the intermolecular dipolar interactions after magnetic dilution. In view of the above evidences, it seems to be clear that the magnetic field is more effective than the dilution in quenching the QTM in **1**.

To better understand the relaxation mechanism, we have attempted to use computed crystal field parameters. The corresponding crystal field Hamiltonian is given as $H_{CF} = B_k^q O_k^q$, where B_k^q is the crystal field parameter while O_k^q is the Steven's operator (Table S10). The axial parameter B_k^q (where k = 0, and q=2) is comparatively larger for Dy2 ion (-1.93) as compared to Dy1 (-1.66) site. This strongly correlates to our computed barrier height and underlines the influence of the ligand field strength in U_{eff}.

Till now, we have only discussed single-ion analysis/behaviour of two individual Dy centres in complex **1**, now we intend to understand its exchange-coupled behaviour. The computed g_{zz} values of the individual Dy_{III} fragments are close to 20. This implies that Dy_{III} - Dy_{III} exchange coupling can be regarded as Ising type. The POLY_ANISO programme was harnessed to fit magnetic susceptibility and magnetization data considering the exchange parameters indicated in Table 3.

Table 3. Fitted exchange coupling constant J_{exch}, computed dipole-dipole interactions $J_{dipolar}$ and the total interaction J_{total} between the *J* ions in complex **1** (all interactions in cm^{-1}). An intermolecular interaction (z*J'*) of -0.003 cm^{-1} was considered.

	Exchange (J, cm^{-1})
J_{exch}	-0.04
$J_{dipolar}$	-0.03
J_{total}	-0.07

The magnetic interactions can be depicted by H = $-Js_{1z1}s_{2z2}$, where s_{1z1} and s_{2z2} represent projections of the effective spin $\tilde{s}$ = ½ of the lowest KDs of the Dy$_{III}$ ions on the principal anisotropy axes. All the parameters of Table 3 were derived with respect to the pseudospin of $\tilde{s}$ = ½ of the Dy$_{III}$ ions. The magnetic coupling J (J_{total}) can be regarded as summation of the exchange interaction (J_{exch}) and magnetic dipole-dipole interaction ($J_{dipolar}$) between the Dy$_{III}$ centres. Using the single-ion based g-tensors for individual Dy$_{III}$ fragments enables precise evaluation of $J_{dipolar}$ (see Table 3). The unknown J_{exch} parameter can be deduced by fitting the experimental magnetic data as mentioned earlier (see Figure S16). Using J_{total} (see Table 3) resulted in nice comparison with respect to experimental magnetic data. The main magnetic axis and local magnetization vectors on the Dy$_{III}$ centres lie in reverse direction in compliance with antiferromagnetic Dy$_{III}$-Dy$_{III}$ coupling within the Lines model (see Figure 4). The main magnetic axes and local magnetization vectors are almost perpendicular (~88° ; see Figure 4) to the Dy1 - Dy2 axis/bond vector. This invokes antiferromagnetic type dipolar interaction between the the Dy$_{III}$ magnetic moments (see Table 3). Despite the opposing alignment of the magnetization vectors, the local magnetization vectors as well as main magnetization vectors on the two Dy sites locate at ~50° with respect to each other. This evokes complete Ising type ground exchange doublet possessing g_{zz}=16.66 (g_{xx}=g_{yy}≈ 10^{-8}) (see Table S11). This implies ground state magnetic moment of 8.33 μ_B which is nearly equal to the magnetic moment of an individual Dy$_{III}$ site indicating weakly coupled Dy centres for

both approaches (see Table 3). Based on the computed $2_2 = 4$ exchange eigenstates local excited states on two Dy centres, we have estimated the magnetic properties of dinuclear Dy_2 complex **1**. Appreciable tunnel splitting ($\Delta_{tun} \approx 10^{-6}$ cm^{-1}; exactly the cut-off value; see Table S11) was noted within ground exchange doublet of **1**harnessing approach-II (see Figure 6). This completely suppresses the relaxation via higher excited exchange doublets and provokes magnetization blockade within ground level itself precluding SMM behaviour contrasting the experimental observation. However, considering the static dc magnetic field application, the first excited exchange doublet is also lying in close proximity (~0.66 cm^{-1}) to the ground level possessing $\Delta_{tun} \approx 10^{-6}$ cm^{-1}(see Table S11 and Figure 6). This close-lying exchange spectrum (expanded within 0.66 cm^{-1}; see Figure 6) and smaller exchange splitting (<1 cm^{-1}) postulates that, experimentally observed barrier inevitably arises from individual Dy_{III} fragments/centres.[32]

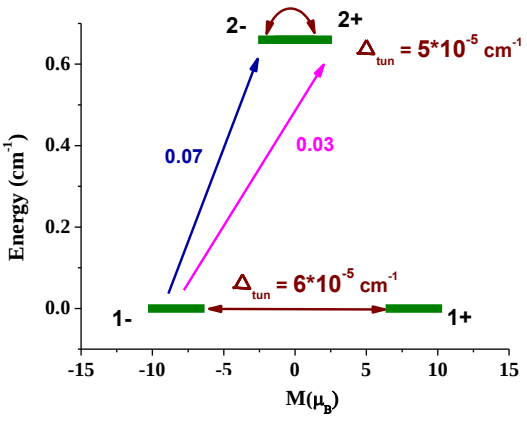

Figure 6.- Low lying exchange spectrum (relative to the energy of the ground state) and position of the magnetization blockade barrier (red dashed line) in Dy_2 complex **1**. The bold green lines indicate exchange states which have been arranged in compliance with the value of its magnetic moment. The brown red arrows (and pertinent values) correspond to tunnelling transitions within ground and first excited exchange doublet. However, blue, pink arrows and corresponding values represent transition magnetic moment matrix elements of spin-phonon relaxation pathways.

For complexes **2** and **3**, the energy separation between KD1 and KD8 are 423 cm-1 and 483 cm-1, respectively, whereas the next excited spin-orbit term is located at 3600 cm-1 for **2** and at 3053 cm-1 for **3** (TablesS8 and S9). In both complexes, the Dy^{III} centres also exhibit a ground state with anisotropy of pure Ising type and large magnetic moments with *g*-tensor values close to an ideally pure M_J = ± 15/2 state (g_z = 20, g_x=g_y = 0). Nevertheless, the axiality of the ground state (KD1) is higher for **3** and in consequence its wavefunction is closer to pure|±15/2>. For these complexes, the axiality decreases from KD1 to KD4 and increase from this latter to KD8, which, like KD1, is almost of Ising type. In both cases, the calculated magnetic moment of the ground state (Figures7 and 8) lies close to the two β-diketonato ligands at opposite sides of each Dy atom,as expected. Qualitative mechanism of relaxation obtained from *ab initio* calculations for **2** and **3** are shown in Figures7 and 8 respectively, together with the computed transverse magnetic moments between the connecting pairs of opposite magnetization.

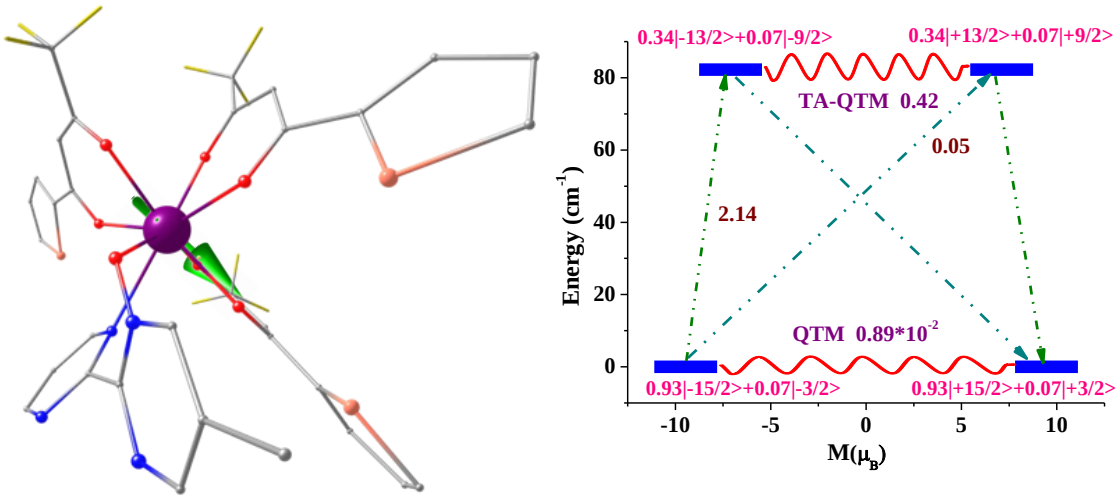

Figure 7.- Crystal structure showing principal anisotropy direction (g_{zz}) of ground state Kramers doublet and *ab initio* computed relaxation mechanism for complex **2.**

For complexes **2** and **3**, QTM in the ground state is not active as the zero transverse magnetic moments are almost negligible (~10^{-2} μ_B, which significantly reduces the

probability of QTM relaxation). In spite of this, experimental results (Figures S9 and S12) show thatat zero field, QTM is the prevailing relaxation process at low temperature. Even in the presence of a dc field of 1 kOe, a small tail below 3 K is observed for complex **2**. To suppress intermolecular dipolar interactions, which favour QTM, the Dy/Y =1/20 diluted versions of **2** and **3** were prepared (**2'** and **3'**). The ac measurements on **2'**and **3'**at zero dc field and 1200 Hz (Figures S17 and S18) clearly show that the tiny tail observed at very low temperature for **2** at 1kOe, due to QTM, vanishes as a result to the drop of the intermolecular dipolar interactions following magnetic dilution. Moreover, the peaks observed in the temperature dependence of the χ''_M signals for the diluted complexes do not appreciably shift with respect to their positions in the neat compounds at 1kOe. In this case, the effect of the dilution on the QTM relaxation is similar to that induced by the magnetic field.

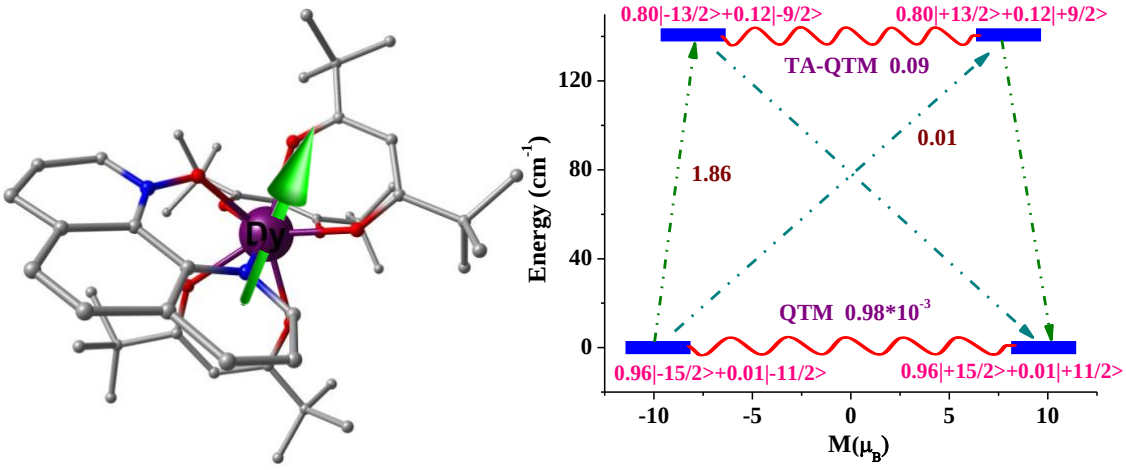

Figure 8.- Crystal structure showing principal anisotropy direction (g_{zz}) of ground state Kramers doublet and *ab initio* computed relaxation mechanism for complex **3.**

The first excited g_{zz} axis for **2** and **3** is notably misaligned with regard to that in the ground state (11.57°and 7.86°, respectively), which underlines that the magnetic relaxation can be operative via first excited state (KD2). This is strongly supported by the calculated

spin-phonon relaxation (Orbach/Raman) contribution from the KD2 (2.14/0.05 and 1.86/0.01, respectively). The relaxation via KD2 is additionally corroborated by significant tunnelling contribution (TA-QTM with transverse magnetic moments of 0.42 μ_B and 0.34, for **2** and **3**, respectively). The ground (KD1)-first excited KD (KD2) gap is computed to be 83 $cm^{-1}$for **2** and 141 cm^{-1} for **3**. We have also computed crystal field parameters for **2** and **3** (Table S12). Negative B_2^0 axial CF parameter corresponds to favourable coordination environment inducing ideal SMM behaviour. The parameter B_2^0 for the Dy in **2** (-0.14) is significantly lower than that Dy in **3** (-0.77) site. This agrees well with the fact that the computed energy barrier for **3** is significantly higher than that shown by **2**.

Comparison of the experimental U_{eff} of complexes **1 – 3** (33 cm^{-1} and 38 cm^{-1} for Dy1 and Dy2 in complex **1** and 49.6 cm^{-1} and 83.4 cm^{-1} for **2** and **3**) with those calculated theoretically reveals that U_{eff} for the latter are, as usual, higher than the former ones. Although the theoretical U_{eff} values for sites Dy1 and Dy2 in complex **1** follow the same trend as the experimental ones, However, they are rather overestimated (109.8 cm^{-1} and 157.2 cm^{-1}, respectively). In view of this, new calculations were performed with approach II (see experimental section) for this complex. Within this new approach, KD1 is found to be slightly less axial (Tables S13, S14) with g_{zz} values somewhat lower than those calculated originally. The energy gap between KD2 and KD1 (U_{calc}) is now 76.29 cm^{-1} (for Dy1 site) and 96.57 cm^{-1} (for Dy2) (table S13, S14 and Figure S20). These values are still higher than experimental but show the same degree of deviation with regard to the experimental ones as those calculated for compounds **2** and **3**. When approach II was applied to complexes **2** and **3**, the theoretical U_{eff} appeared to be underestimated, particularly complex **2**, which exhibits a value much lower than that obtained experimentally. Thus, these results have not been considered in this work. It seems that

approach II is more adequate for the dinuclear complex **1**, whereas approach I turns out to be more suitable mononuclear complexes, specifically for compound **2**. The calculated magnetic moments of the ground state for Dy1 and Dy2 sites and the SINGLE_ANISO computed crystal fields parameters calculated for **1** with approach II are quite similar to those calculated initially and thus do not deserve to be further discussed. This information has been included in the supporting information.

In general, to generate a high energy barrier, leading to slow magnetic relaxation and SMM behaviour, a ground state with high M_J is mandatory. In the case of Dy^{III} ion, this condition can be attained with an axial coordination environment that enhances the electron density close to the axis. For eight-coordinated complexes with almost equivalent donor atoms and similar Dy-donor distances, an axially elongated square antiprism coordination sphere (D_{4d}) favours the existence of a large energy barrier for magnetization reversal with almost pure M_J wave function in the ground state. Deviations from this symmetry provoke mixing of M_J wavefunctions in the ground doublet state, which favours the fast quantum tunnelling of the magnetization that reduces or fully eliminates the energy barrier. Low symmetry Dy^{III} complexes with different ligands and Dy-O distances generally exhibit easy axis anisotropy in the ground KD leading to a barrier for magnetization reversal and slow relaxation of the magnetization. In these cases and to reduce the repulsion between the electron density of the M_J = 15/2 Dy^{III} ground KD (which has an oblate disc shape) with the closest coordinated atoms, the disc shaped electron density is accommodated almost perpendicular to the shortest Dy-O bond distances,[1b] so that the magnetic moment (which is perpendicular to the electron density disc)lies in the direction of the shortest Dy-O bonds. Nevertheless, in most cases, the ground state wave functions is not pure $|\pm 15/2>$ but a little bit mixed with some lower M_J wave functions and so the complexes exhibit unwanted fast QTM at zero field that

decreases the temperature at which magnetic hysteresis is observed. In view of these considerations, a good strategy to access to SMM complexes in eight-coordinated Dy^{III} would be that of creating an axially elongated crystal field around the Dy^{III} center (preferably of square prismatic geometry) by placing the ligands with the shorter Dy-O distances at opposite sides of each Dy atom and the remaining atoms at the equatorial plane. Complexes **1**-**3** obey this criterium as they have two β-diketonato ligands at opposite sides of each Dy atom,while the remaining positions in the equatorial plane are occupied by the oxygen atoms of the other β-diketonato bidentate ligand and the N,N or N,O atoms belonging to the N-oxide ligands. This configuration generates, as indicated elsewhere, an appropriate axial crystal field, because the Dy-O bond distances belonging to the β-diketonato ligand are the shortest ones, and similar to the Dy-O distance of the N-oxide group. The two β-diketonato ligands at opposite sides of each Dy^{III}atom creates a "pseudo axis" with the magnetic moment lying close to it.Theoretical and experimental studies have revealed that the distortion of the local coordination environment of the Dy^{III} ion from an ideal geometry can significantly affects the magnetization relaxation dynamics.[26b,33,34] In fact, for eight coordinated Dy^{III} SMM complexes, the distortion from square antiprismatic to triangular dodecahedral geometries promotes a reduction of the energy barrier.[35]The calculated energy barriers (energy gap between KD1 and KD2 doublets) for the Dy^{III} ions linked to the N,O bidentate part of the ligands in complexes **1**-**3** follow this trend as *U* values decrease with the distortion from the square antiprism geometry quantified by the shape measures parameter (S): 0.55 (141 cm^{-1}) for **3**, 0.79 (82.3 cm^{-1}) for **2** and 1.70 (76 cm^{-1}, approach II) for **1**. Although rather smaller that the calculated values, the experimental ones follow the same order 83.8 cm^{-1} for **3**, 49.6 cm^{-1} for **2** and 33 cm^{-1} for **1**.

Pulse Magnetization Measurements

In order to confirm the SMM properties of **1**-**3** we have measured the magnetization curve in a full cycle pulsed magnetic field at 0.4 K,[36] with maximum fields of 0.84, 2.6, 5.2 and 10.4 T. It should be noted that the sweep rate depends on the maximum field and therefore is higher for 10.4 T (4.2 T/ms). Magnetization curves (Figure 9 for compound **1** and Figure 10 for compound **2** and **3)** show large hysteresis loops, a sharp reversal at around zero field and saturations at high fields. The hysteresis increases with increasing the sweeping rate, which is typical of SMMs. The reduction for the saturation moment per Dy ion from the expected value (10μβ/f.u.) is due to powder sample average. The sharp reversal around zero indicates that that there is an adiabatic magnetization reversal presumably caused by the fast tunneling process with a small tunneling gap. The possible cause of the gap is inferred to be hyperfine interactions and/or transverse components of the magnetization by the low symmetry around Dy^{III} ion. Contribution of weak inter-molecular interactions should less significant, because the sharp reversals are observed in common for three complexes. This means that the pulse magnetization behaviour for **1-3** is a single molecule property.

To examine the origin of the loop, the differential magnetization dM/dB is plotted (Figure 9 right, Figure10 and Figure S21) .

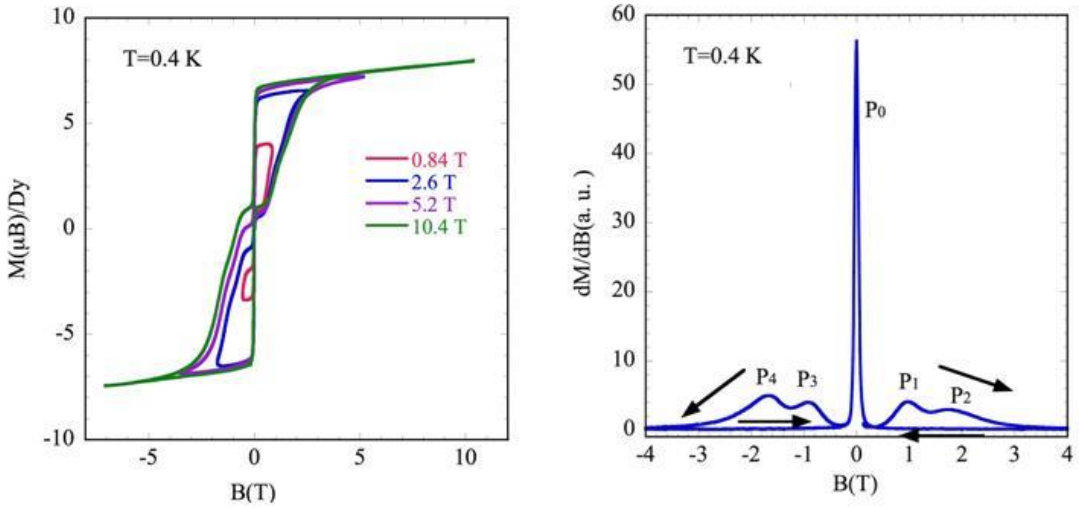

Figure 9.- Pulsed-field magnetization curves at maximum fields of 0.84 T, 2.6 T, 5.2 T and 10.4 T for (Left) and differential of magnetization measured at 0.4 K. (right) for compound **1**.

For 1, in the initial up sweep, the magnetization first increases slowly and then it shows two peaks P1 and P2. These two peaks correspond to two steps in the magnetization curve. In the down sweep from the magnetic field peak to the zero field, the dM/dH is very small and the magnetization curve is nearly flat. The characteristic loop structure in the positive field side shows that there are two barriers with different magnitudes and thus the release field of the trapped magnetization splits into two. The existence of two barriers is also found as double peak structure in the χ". After the sharp drop of the magnetization at around zero field, the magnetization stays around zero. Then the magnetization curve in the negative field side is symmetric to that in the positive field side. In the initial sweep from the zero field to the negative maximum, we found two peaks P3 and P4 in dM/dB.

The sweep rate dependence of peaks P1~P4 (Figure S22) indicates that the magnetization behaviour is symmetric for the magnetic field reversal as is found in the magnetization curve. There is slight sweep rate dependence of the peak field. It is presumably caused by the balance between the thermal relaxation time and the short sweeping time. The

occurrence of two steps magnetization curve in the dinuclear complex **1** and the presence of only one step for the mononuclear complexes **2** and **3** (Figure 9) point out that the two barriers in complex **1** can be caused by the sizable magnetic coupling between two Dy ions. Nevertheless, these two barriers could also appear due to the non-equivalence Dy1 and Dy2 when magnetic coupling through the bridging ligand is negligible.

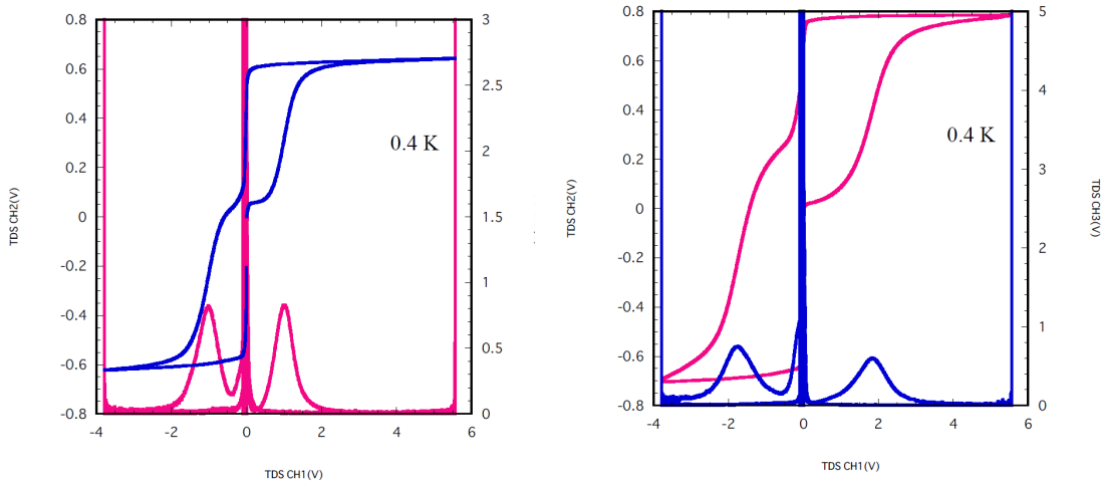

Figure 10.- Pulsed-field magnetization curves at maximum field of 10.4 T and differential of magnetization measured at 0.4 K for compound **2** (left) and **3** (right).

It should be remarked that the hysteresis is larger for **3** than for **2**, which matches well with the fact that the theoretical and experimental U_{eff} values for the former are significant larger that for the latter.

Conclusions

The dissymmetric bridging ligand 4-methyl-bipyrimidine-2-N-oxide (mbpymNO) allows designing thr non-symmetric dinuclear Dy(III) complex **1** exhibiting two different Dy1 and Dy2 sites, which are related to the N^O and N^N chelating sites of the ligand, respectively. Ac magnetic measurements reveal the existence of two different slow

magnetic relaxation processes associated to Dy1 and Dy2 with effective thermal energy barriers values of 47.8 (FR) and 54.7 K (SR) respectively. The fact that Dy1 shows a higher distortion from an ideal D_{4d} geometry than Dy2 could justify because U_{eff} (Dy1) < U_{eff} (Dy2). Ab initio studies indicate that the ground state of both sites is of an Ising type and support the existence of two relaxation processes with computed energy gaps between the ground and first excited Kramers doublets of 76 cm^{-1}(Dy1) and 97 cm^{-1}(Dy2). Additionally, two mononuclear SMM complexes were prepared from the mbpymNO (**2**) and phenNO (**3**) ligands. In both cases, the Dy(β-diketonate)$_3$ moieties are chelated to the N^O coordination site of the ligands and SMM is observed with U_{eff} values of 49.6 cm^{-1} for **2** and 83.4 cm^{-1} for **3**. Analysis of the structural and SMM properties of the Dy(III) units linked to the N^O site of the ligands in **1 – 3**, demonstrate that U_{eff} increase as the symmetry of the Dy(NO_7) coordination sphere approaches to an ideal D_{4d}symmetry. Pulse magnetization measurements support the SMM behaviour of **1**-**3**. As expected, differential magnetization dM/dB curves for the dinuclear Dy_{III} complex **1** exhibit hysteresis loops with double step structure, whereas those for the mononuclear complexes **2** and **3** only display one step.

Acknowledgements

I. F. D. O., J. M. H. E. R. and E. C. are grateful to Ministerio de Economía y Competitividad (MINECO) and EU Feder Funds (Projects CTQ2014-56312-P and CTQ2015-64579-C3-1-P), the Junta de Andalucía (FQM-195 and the Project of Excellence P11-FQM-7756) and the University of Granada for financial support. A part of this work has been made at HFLSM, IMR, Tohoku University. I. F. D.O.also acknowledges support by COLABS.G.R. and T. G. would like to thank DST-SERB

(EMR/2014/00024) for funding. E.R. thanks Generalitat de Catalunya for an ICREA Academia award.

References

1.- Some reviews: (a) Gatteschi, D.; Sessoli, R.; Villain, J.; *Molecular Nanomagnets;* Oxford University Press, Oxford, U.K., **2006**. (b) Rinehart, J. D.; Long, J. R. Exploiting single-ion anisotropy in the design of f-element single-molecule magnets. *Chem. Sci.***2011**, *2*,2078-2085. (c) Guo, Y. N.; Xu, G. F.; Guo, Y.; Tang, J. Relaxation dynamics of dysprosium(iii) single molecule magnets. *Dalton Trans.* **2011**, *40*, 9953-9963. (d) Sorace, L.; Benelli, C.; Gatteschi, D. Lanthanides in molecular magnetism: old tools in a new field. *Chem. Soc. Rev*. **2011**, *40*, 3092-3104. (e) Luzon, J.; Sessoli, R. Lanthanides in molecular magnetism: so fascinating, so challenging. *Dalton Trans*. **2012**, *41*, 13556-13567. (f) Clemente-Juan, J. M.; Coronado, E.; Gaita-Ariño, A. Magnetic polyoxometalates: from molecular magnetism to molecular spintronics and quantum computing. *Chem. Soc. Rev.***2012**, *41*, 7464-7478. (g) Woodruff, D. N.; Winpenny, R. E. P.; Layfield, R. A. Lanthanide Single-Molecule Magnets. *Chem. Rev*. **2013**, *113*, 5110-5148. (h) Zhang, P.; Guo, Y.-N.; Tang, J. Recent advances in dysprosium-based single molecule magnets: Structural overview and synthetic strategies. *Coord. Chem. Rev.***2013**, *257*, 1728-1763. (i)Layfield, R. A.; Murugesu, M. (eds), *Lanthanides and Actinides in Molecular Magnetism*, Wiley-VCH, Weinheim, Germany, 2015.(j) Tang, J.; Zhang, P. *Lanthanide Single Molecule Magnets*, Springer-Verlag Berlin Heidelberg, 2015. (k) Habib, F.; Murugesu, M. Lessons learned from dinuclear lanthanide nano-magnets. *Chem. Soc. Rev.* **2013**, *42*, 3278-3288. (l) Layfield, R. A. Organometallic Single-Molecule Magnets. *Organometallics* **2014**, *33*, 1084-1099. (m) Wang, B. W.; Gao, S.; *The Rare Earth Elements, Fundamental and Applications*, Ed. D. A. Atwood, John Wiley

and sons, 2012. (n) Sessoli, R.; Powell, A. K. Strategies towards single molecule magnets based on lanthanide ions. *Coord. Chem. Rev.***2009**, *253*, 2328-2341. (o) Andruh, M.; Costes, J. P.; Diaz, C.; Gao, S. 3d−4f Combined Chemistry: Synthetic Strategies and Magnetic Properties. *Inorg. Chem*. **2009**, *48*, 3342-3359. (p) Brechin, E. K "*Molecular Magnets*" themed issue; *Dalton Trans*. **2010**, *39*, 4671. (q) Sharples, J. W.;Collison, D. The coordination chemistry and magnetism of some 3d–4f and 4f amino-polyalcohol compounds.*Coord. Chem. Rev.***2014**, *260*, 1-20. (r) Rosado, L.; Sañudo, E. C. Heterometallic 3d-4f single-molecule magnets. *Dalton Trans*.**2015**,***44***, 8771-8780. (s) Craig, G. A.; Murrie, M. 3d single-ion magnets. *Chem. Soc. Rev.* **2015**, *44*, 2135-2147. (t) Bartolomé, J.; Luis, F.; Fernández, J. F. *Molecular Magnets: Physics and Applications*, Ed. Springer-Verlag, Berlin-Heidelberg, 2014.(u) Aromí, G.; Brechin, E. K. *Struct. Bond*. **2006**, *122*, 1.(v) Bagai, R.; Christou, G. The Drosophila of single-molecule magnetism: $[Mn_{12}O_{12}(O_2CR)_{16}(H_2O)_4]$. *Chem. Soc. Rev.***2009**, *38*, 1011-1026. (w) Liddle, S. T.; van Slageren, J. Improving f-element single molecule magnets.*Chem. Soc. Rev.*, 2015, **44**, 6655-6669. (y) Frost, J. M.; Harriman, K. L. M.; Murugesu, M. The rise of 3-d single-ion magnets in molecular magnetism: towards materials from molecules. *Chem. Sci.***2016**, *7*, 2470-2491. (z) Harriman, K. L. M.; Murugesu, M. An Organolanthanide Building Block Approach to Single-Molecule Magnets.*Acc. Chem. Res.* **2016**, *49*, 1158-1167.

2.-(a) Bogani, L.; Wernsdorfer, W. Molecular spintronics using single-molecule magnets. *Nat. Mater*.**2008**, *7*, 179-186.(b) Vincent, R.; Klyatskaya, S.; Ruben, M.; Wernsdorfer, W.; Balestro, F. Electronic read-out of a single nuclear spin using a molecular spin transistor. *Nature***2012**, *488*, 357-360. (c) Ganzhorn, M.; Klyatskaya, S.; Ruben, M.; Wernsdorfer, W. Strong spin-phonon coupling between a single-molecule magnet and a carbon nanotube nanoelectromechanical system. *Nat. Nano*. **2013**, *8*, 165-169. (d) Jenkins, M.; Hümmer, T.; Martínez-Pérez, M. J.; García-Ripoll, J.; Zueco, D.; Luis, F.

Coupling single-molecule magnets to quantum circuits. *New. J. Phys.***2013**, *15*, 095007. (e) Dediu, V. A.; Hueso, L. E.; Bergenti, I.; Taliani, C. Spin routes in organic semiconductors. *Nat. Mater*. **2009**, *8*, 707-716. (f) Prezioso, M.; Riminucci, A.; Graziosi, P.; Bergenti, I.; Rakshit, R.; Cecchini, R.; Vianelli, A.; Borgatti, F.; Haag, N.; Willis, M.; Drew, A. J.; Gillin, W. P.; Dediu, V. A. A Single-Device Universal Logic Gate Based on a Magnetically Enhanced Memristor.*Adv. Mater*. **2013**, *25*, 534-538. (g) Mannini, M.; Pineider, F.; Danieli, C.; Totti, F.; Sorace, L.; Sainctavit, P.; Arrio, M.-A.; Otero, E.; Joly, L.; Cezar, J. C.; Cornia, A.; Sessoli, R. Quantum tunnelling of the magnetization in a monolayer of oriented single-molecule magnets. *Nature***2010**, *468*, 417-421. (h) Thiele, S.; Balestro, F.; Ballou, R.; Klyatskaya, S.; Ruben, M.; Wernsdorfer, W. Electrically driven nuclear spin resonance in single-molecule magnets. *Science***2014**, *344*, 1135-1138. i)Cornia, A.; Seneor, P. Spintronics: The molecular way. *Nat. Mater*. **2017**, *16*, 505-506. j) Lumetti, S.; Candini, A.; Godfrin, C.; Balestro, F.; Wernsdorfer, W.; Klyatskaya, S.; Ruben, M.; Affronte, M. Single-molecule devices with graphene electrodes. *Dalton Trans*. **2016**, *45*, 16570-16574.

3.- (a) Rocha, A. R.; García-Suárez, V. M.; Bailey, S. W.; Lambert, C. J.; Ferrerand, J.; Sanvito, S. Towards molecular spintronics. *Nat. Mater*.**2005**, *4*, 335-339.(b) Affronte, M. Molecular nanomagnets for information technologies. *J. Mater. Chem*. **2009**, *19*, 1731-1737.

4.- Sessoli, R.; Boulon, M.-E.; Caneschi, A.; Mannini, M.; Poggini, L.; Wilhelm, F.; Rogalev, A. Strong magneto-chiral dichroism in a paramagnetic molecular helix observed by hard X-rays. *Nat. Phys*.**2015**, *11*, 69-74.

5.-(a) Leuenberger, M. N.; Loss, D. Quantum computing in molecular magnets. *Nature***2001**, *410*, 789-793. (b) Ardavan, A.; Rival, O.; Morton, J. J. L.; Blundell, S. J.; Tyryshkin, A. M.; Timco, G. A.; Winpenny, R. E. P. Will Spin-Relaxation Times in

Molecular Magnets Permit Quantum Information Processing?.*Phys. Rev. Lett.***2007**, *98*, 057201. (c) Stamp, P. C. E.; Gaita-Ariño, A. Spin-based quantum computers made by chemistry: hows and whys. *J. Mater. Chem*. **2009**, *19*, 1718-1730. (d) Martínez-Pérez, M. J.; Cardona-Serra, S.; Schlegel, C.; Moro, F.; Alonso, P. J.; Prima-García, H.; Clemente-Juan, J. M.; Evangelisti, M.; Gaita-Ariño, A.; Sesé, J.; Van Slageren, J.; Coronado, E.; Luis, F. Gd-Based Single-Ion Magnets with Tunable Magnetic Anisotropy: Molecular Design of Spin Qubits. *Phys. Rev. Lett.* **2012**, *108*, 247213.e)Ghirri, A.; Troiani, F.; Affronte, M. Molecular Spins in the Context of Quantum Technologies. *Magnetochemistry* **2017**, *3*(1), 12.

6.- (a) Chen, Y.; Liu, J.; Ungur, L.; Liu, J.; Li, Q.;Wang, L.; Ni, Z.; Chibotaru, L. F.; Chen, X.; Tong, M. Symmetry-Supported Magnetic Blocking at 20 K in Pentagonal Bipyramidal Dy(III) Single-Ion Magnets. *J. Am. Chem. Soc.*, **2016**, *138*, 2829-2837. (b) Gupta, S. K.; Rajeshkumar, T.; Rajaraman, G.; Murugavel, R. An air-stable Dy(III) single-ion magnet with high anisotropy barrier and blocking temperature. *Chem. Sci.* **2016,** *7*, 5181-5191. (c) Liu, J.; Chen, Y.; Jia, J.; Liu, J.; Vieru, V.; Ungur, L.; Chibotaru, L. F.; Lan, Y.; Wernsdorfer, W.; Gao, S.; Chen, X.; Tong, M. A Stable Pentagonal Bipyramidal Dy(III) Single-Ion Magnet with a Record Magnetization Reversal Barrier over 1000 K. *J Am. Chem Soc.*, **2016**, *138*, 5441-5450. (d) Gregson, M.; Chilton, N. F.; Ariciu, A-M.; Tuna, F.; Crowe, I. F.; Lewis, W.; Blake, A. J.; Collison, D.; McInnes, E. J. L.; Winpenny, R. E. P.; Liddle, S. T. A monometallic lanthanide bis(methanediide) single molecule magnet with a large energy barrier and complex spin relaxation behavior. *Chem. Sci.***2016**, *7*, 155-165. (e) Ding, Y.-S.; Chilton, N. F.; Winpenny, R. E. P.; Zheng, Y.-Z. On Approaching the Limit of Molecular Magnetic Anisotropy:A Near-Perfect Pentagonal Bipyramidal Dysprosium(III) Single-Molecule Magnet. *Angew. Chemie Int. Ed*. **2016**, *55*, 16071-16074. (f) Chen, Y.C; Liu, J.L.; Lan, Y.; Zhong, Z.

Q.;Mansikkamäki, A.; Ungur, L.;Jia, J. H.;Chibotaru, L. F.; Han, J. B.;Wernsdorfer, W.; Chen, X. M.; Tong, M. L.Dynamic Magnetic and Optical Insight into a High Performance Pentagonal Bipyramidal DyIII Single-Ion Magnet.*Chem. - Eur. J.***2017**, *23*, 5708-5715.g) Guo, F.-S.; Day, B. M.; Chen, Y.-C.; Tong, M.-L.; Mansikkamäki, A.; Layfield, R. A.; A Dysprosium Metallocene Single-Molecule Magnet Functioning at the Axial Limit. *Angew. Chem. Int. Ed.***2017**, *56*, 11445-11449. h) Goodwin, C. A. P.; Ortu, F.; Reta, D.; Chilton, N. F.; Mills, D. P. Molecular magnetic hysteresis at 60 kelvin in dysprosocenium. *Nature*, **2017**, *548*, 439-442.

7.- (a) Ruiz, J.; Mota, A. J.; Rodríguez-Diéguez, A.; Titos, S.; Herrera, J. M.; Ruiz, E.; Cremades, E.; Costes J.P., Colacio, E. Field and dilution effects on the slow relaxation of a luminescent DyO_9 low-symmetry single-ion magnet.*Chem. Commun*.**2012**, *48*, 7916-7918. (b) Das, S.; Dey, A.; Biswas, S.; Colacio, E.; Chandrasekhar, V. Hydroxide-Free Cubane-Shaped Tetranuclear [Ln_4] Complexes. *Inorg.Chem.* **2014**, *53*, 3417-3426.

8.- (a) Xue, S.; Ungur, L.; Gao, Y.-N.; Tang, J.; Chibotaru, L. F. Field-induced Multiple relaxation mechanism of $Co^{III}_2Dy^{III}_2$ compound with the Dysprossium ion in a Low-Symmetrical Environment. *Inorg. Chem.***2014**, *53*, 12658-12663. (b) Habib, F.; Korobkov, I.; Murugesu, M. Exposing the intermolecular nature of the second relaxation pathway in a mononuclear cobalt(II) single-molecule magnet with positive anisotropy. *Dalton Trans*. **2015**, *44*, 6368-6373.

9.- (a) Yi, X.; Calvez, G.; Daiguebonne, C.; Guillou, O.; Bernot, K. Rational Organization of Lanthanide-Based SMM Dimers into Three-Dimensional Networks. *Inorg. Chem*. **2015**, *54*, 5213-5219. (b) Pointillart, F.; Le Guennic, B.; Golhen, S.; Cador, O.; Ouahab, L. Slow magnetic relaxation in radical cation tetrathiafulvalene-based lanthanide(III) dinuclear complexes. *Chem. Commun.***2013**, *49*, 11632-11634. (c) Pointillart, F.; Le Guennic, B.; Cauchy, T.; Golhen, S.; Cador, O.; Maury, O.; Ouahab, L. A Series of

Tetrathiafulvalene-Based Lanthanide Complexes Displaying Either Single Molecule Magnet or Luminescence—Direct Magnetic and Photo-Physical Correlations in the Ytterbium Analogue.*Inorg. Chem.***2013**, *52*, 5978-5990. (d) Han, T.; Shi, W.; Zhang, X. P.; Li, L. L.; Cheng, P. A Family of Binuclear Dysprosium(III) Radical Compounds with Magnetic Relaxation in ON and OFF States. *Inorg. Chem.***2012**, *51*, 13009-13016. (e) Eliseeva, S. V.; Ryazanov, M.; Gumy, F.; Troyanov, S. I.; Lepnev, L. S.; Bünzli, J. C. G.; Kuzmina, N. P. Dimeric Complexes of Lanthanide(III) Hexafluoroacetylacetonates with 4-Cyanopyridine N-Oxide: Synthesis, Crystal Structure, Magnetic and Photoluminescent Properties. *Eur. J. Inorg. Chem.*, **2006**, *2006*, 4809-4820. f) Murashima, K.; Karasawa, S.; Yoza, K.; Inagaki, Y.; Koga, N. 3- and 4-([α]-diazobenzyl)pyridine-N-oxides as photoresponsive magnetic couplers for 2p-4f heterospin systems: formation of carbene-Tb^{III} and carbene-Dy^{III} single-molecule magnets. *Dalton Trans.***2016**, *45*, 7067-7077.(g) Pointillart, F.; Le Guennic, B.; Maury, O.; Golhen, S.; Cador, O.; Ouahab, L. Lanthanide Dinuclear Complexes Involving Tetrathiafulvalene-3-pyridine-N-oxide Ligand: Semiconductor Radical Salt, Magnetic, and Photophysical Studies. *Inorg. Chem.***2013**, *52*, 1398-1408. (h) Pointillart, F.; Le Gal, Y.; Golhen, S.; Cador, O.; Ouahab, L. Single-Molecule Magnet Behaviour in a Tetrathiafulvalene-Based Electroactive Antiferromagnetically Coupled Dinuclear Dysprosium(III) Complex. *Chem. – Eur. J.*,**2011**, *17*, 10397-10404. (i) Kiefl, E.;Mannini, M.;Bernot, K.;Yi, X.;Amato, A.; Leviant, T.;Magnani, A.;Prokscha, T.;Suter, A.;Sessoli, R.; Salman, Z. Robust Magnetic Properties of a Sublimable Single-Molecule Magnet. *ACS Nano***2016**, *10*, 5663-5669. j) Zhu W.; Xiong X.; Gao C.; Li S.; Zhang Y.; Wang J.; Zhang C.; Powell A.K., Gao S., A family of one-dimensional lanthanide complexes bridged by two distinct carboxylate ligands with the Dy analogue displaying magnetic relaxation behaviour, *Dalton Trans.* **2017**, 46, 14114-14121.

10.- (a) Wang, Y.-L.; Ma, Y.; Yang, X.; Tang, J.; Cheng, P.; Wang, Q.-L.; Li, L.-C.; Liao, D.-Z. Syntheses, Structures, and Magnetic and Luminescence Properties of a New DyIII-Based Single-Ion Magnet.*Inorg. Chem*. **2013**, *52*, 7380-7386. (b) Chen, G.-J.; Gao, C.-Y.; Tian, J.-L.; Tang, J.; Gu, W.; Liu, X.; Yan, S.-P.; Liao, D.-Z.; Cheng, P. Coordination-perturbed single-molecule magnet behaviour of mononuclear dysprosium complexes. *Dalton Trans*. **2011**, *40*, 5579-5583. (c) Chen, G.-J.; Guo, Y.-N.; Tian, J.-L.; Tang, J.; Gu, W.; Liu, X.; Yan, S.-P.; Cheng, P.; Liao, D.-Z. Enhancing Anisotropy Barriers of Dysprosium(III) Single-Ion Magnets. *Chem. - Eur. J.***2012**, *18*, 2484-2487. (d) Cen,P.-P.; Zhang, S.;Liu, X.-Y.;Song, W.-M.;Zhang, Y.-Q.; Xie, G.;Chen, S.-P. Electrostatic Potential Determined Magnetic Dynamics Observed in Two Mononuclear β-Diketone Dysprosium(III) Single-Molecule Magnets. *Inorg. Chem.***2017**, *56*, 3644-3656. (e) Tong, Y.-Z.; Gao, C. Wang, Q.-L.; Wang, B.-W.; Gao, S.;Cheng, P.; Liao, D.-Z. Two mononuclear single molecule magnets derived from dysprosium(III) and tmphen (tmphen =3,4,7,8-tetramethyl-1,10-phenanthroline). *Dalton Trans.***2015**, *44*, 9020-9026. (f) Sun, W.-B.; Yan, B.; Ji, L.-H.; Wang, B.-W.; Yang, Q.; Cheng, X.; Li, H.-F.; Chen, P.; Wang, Z.-M.; Gao, S. Dinuclear dysprosium SMMs bridged by a neutral bipyrimidine ligand: two crystal systems that depend on different lattice solvents lead to a distinct slow relaxation behavior. *Dalton Trans*. **2016**, *45*,8790-8794. (g) Yu, W.; Schramm, F.; Moreno Pineda, E.; Lan, Y.; Fuhr, O.; Chen, J.; Isshiki, H.; Wernsdorfer, W.; Wulfhekel, W.; Ruben, M. Single-molecule magnet behavior in 2,2'-bipyrimidine-bridgeddilanthanide complexes**,** *Beilstein J. Nanotechnol.* **2016,** *7*, 126-137.

11.-Corey, E. J.; Borror, A. L.; Foglia, T. Transformations in the 1,10-Phenanthroline Series. *J. Org. Chem.*, **1965**, *30*, 288-290.

12.- Rodríguez-Dieguez, A.; Kivekas, R.; Sakiyama, H.; Debdoubid, A.; Colacio, E. A novel 3D cyano-bridged mixed-valence CoII/CoIII canted antiferromagnet constructed

from defective cubanes. Synthesis, X-ray structure and magnetic properties.*Dalton Trans*. **2007**, *0*, 2145–2149

13.- Sheldrick, G. M. A short history of SHELX.*Acta Crystallogr*. *Sect. A*, **2007**, *64*, 112-122.

14.-Dolomanov, O. V.; Bourhis, L. J.; Gildea, R. J.; Howard, J. A. K.;Puschmann, H. OLEX2: A complete structure solution, refinement and analysis program. *J. Appl. Crystallogr*.**2009**, *42*, 339–341.

15.- Nojiri, H.; Choi, K.-Y.; Kitamura, N. Manipulation of the quantum tunneling of nanomagnets by using time-dependent high magnetic fields. *J. Magn. Magn.Mater*.**2007**, *310*, 1468-1472.

16.- (a) Aquilante, F.; Autschbach, J.; Carlson, R. K.; Chibotaru, L. F.; Delcey, M. G.; De Vico, L.; Fdez. Galván, I.; Ferré, N.; Frutos, L. M.; Gagliardi, L.; Garavelli, M.; Giussani, A.; Hoyer, C. E.; Li Manni, G.; Lischka, H.; Ma, D.; Malmqvist, P. Å.; Müller, T.; Nenov, A.; Olivucci, M.; Pedersen, T. B.; Peng, D.; Plasser, F.; Pritchard, B.; Reiher, M.; Rivalta, I.; Schapiro, I.; Segarra-Martí, J.; Stenrup, M.; Truhlar, D. G.; Ungur, L.; Valentini, A.; Vancoillie, S.; Veryazov, V.; Vysotskiy, V. P.; Weingart, O.; Zapata, F.; Lindh, R. Molcas 8: New capabilities for multiconfigurational quantum chemical calculations across the periodic table. *J. Comput. Chem.* **2016**, *37*, 506-541. (b) Aquilante, F.; De Vico, L.; Ferre, N.; Ghigo, G.; Malmqvist, P. A.; Neogrady, P.; Pedersen, T. B.; Pitonak, M.; Reiher, M.; Roos, B. O.; Serrano-Andres, L.; Urban, M.; Veryazov, V.; Lindh, R. MOLCAS 7: The Next Generation. *J. Comput. Chem.* **2010,***31*, 224-247. (c) Duncan, J. A. Molcas 7.2. *J. Am. Chem. Soc.* **2009**, *131*, 2416-2416;(d) Veryazov, V.; Widmark, P. O.; Serrano-Andres, L.; Lindh, R.; Roos, B. O. 2MOLCAS as a development platform for quantum chemistry software. *Int. J. Quantum Chem.* **2004**, *100*, 626-635. (e) Karlstrom, G.; Lindh, R.; Malmqvist, P. A.; Roos, B. O.; Ryde, U.;

Veryazov, V.; Widmark, P. O.; Cossi, M.; Schimmelpfennig, B.; Neogrady, P.; Seijo, L. MOLCAS: a program package for computational chemistry. *Comput.Mater. Sci.* **2003**, *28*, 222-239.

17.- Chibotaru, L. F.; Ungur, L. Ab initio calculation of anisotropic magnetic properties of complexes. I. Unique definition of pseudospin Hamiltonians and their derivation. *J.Chem. Phys*. **2012**, *137*, 064112/1-064112/22.

18.- (a) Langley, S. K.; Ungur, L.; Chilton, N. F.; Moubaraki, B.; Chibotaru, L. F.; Murray, K. S. Single-Molecule Magnetism in a Family of {CoIII2DyIII2} Butterfly Complexes: Effects of Ligand Replacement on the Dynamics of Magnetic Relaxation. *Inorg. Chem.***2014**, *53*, 4303-4315. (b) Habib, F.; Luca, O. R.; Vieru, V; Shiddiq, M.; Korobkov, I.; Gorelsky, S. I.; Takase, M. K.; Chibotaru, L. F.; Hill, S.; Crabtree, R. H.; Murugesu, M. Influence of the Ligand Field on Slow Magnetization Relaxation versus Spin Crossover in Mononuclear Cobalt Complexes. *Angew. Chem. Int. Ed*. **2013**, *52*, 11290-11293.

19.-Roos, B. O.; Lindh, R.; Malmqvist, P. A.; Veryazov, V.; Widmark, P. O.; Borin, A. C. New Relativistic Atomic Natural Orbital Basis Sets for Lanthanide Atoms with Applications to the Ce Diatom and LuF_3. *J. Phys. Chem. A***2008**, *112*, 11431-11435.

20.- Koch, H.; Sánchez de Merás, A.; Pedersen, T. B. Reduced scaling in electronic structure calculations using Cholesky decompositions. *J. Chem. Phys.* **2003,***118*, 9481-9484.

21. Ungur, L.; Chibotaru, L. F. *POLY_ANISO program*, KU Leuven:Belgium, **2007**.

22.- (a) Ungur, L.; Thewissen, M.; Costes, J.-P.; Wernsdorfer, W.; Chibotaru, L. F. Interplay of Strongly Anisotropic Metal Ions in Magnetic Blocking of Complexes. *Inorg. Chem.* **2013**, *52*, 6328-6337. (b) Feltham, H. L. C.; Lan, Y.; Klöwer , F.; Ungur, L.; Chibotaru, L. F.; Powell, A. K.; Brooker, S. A Non-sandwiched Macrocyclic

Monolanthanide Single-Molecule Magnet: The Key Role of Axiality. *Chem. – Eur. J.* **2011,***17*, 4362-4365. (c) Ungur, L.; Chibotaru, L. F. Magnetic anisotropy in the excited states of low symmetry lanthanide complexes. *Phys. Chem. Chem. Phys.* **2011,***13*, 20086-20090.

23.- Llunell, M.; Casanova, D.; Cirera, J.; Bofill, J. M.; Alemany, P.; Alvarez, S.; Pinsky, M; Avnir, D. *SHAPE v1.1b program*, Barcelona, **2005.**

24.-Bi, Y.; Guo, Y. –N.; Zhao, L.; Guo, Y.; Lin, S. –Y.; Jiang, S. –D.; Tang, J.; Wang, B. –W.; Gao, S. Capping Ligand Perturbed Slow Magnetic Relaxation in Dysprosium Single-Ion Magnets. *Chem. - Eur. J.***2011**, *17*, 12476 – 12481.

25.- Chilton, N.F. *CCFIT program* /http://www.nfchilton.com/software.html, **2014**.

26.- a) Feltham, H. L. C.; Lan, Y.; Klöwer, F.; Ungur, L.; Chibotaru, L. F.; Powell, A. K.; Brooker, S. A Non-sandwiched Macrocyclic Monolanthanide Single-Molecule Magnet: The Key Role of Axiality. *Chem. - Eur. J.***2011**, *17*, 4362-4365. b) Costes, J. P.; Titos-Padilla, S.; Oyarzabal, I.; Gupta, T.; Duhayon, C.; Rajaraman, G.; Colacio, E. Analysis of the Role of Peripheral Ligands Coordinated to ZnII in Enhancing the Energy Barrier in Luminescent Linear Trinuclear Zn-Dy-Zn Single-Molecule Magnets. *Chem. - Eur. J.* , **2015**, 21, 15785-15796.

27.- (a) Rinehart, J. D.; Long, J. R. Exploiting single-ion anisotropy in the design of f-element single-molecule magnets. *Chem. Sci*. **2011**, *2*, 2078−2085. (b) Kajiwara, T.; Nakano, M. K.; Takaishi, S.; Yamashita, M. Structural Design of Easy-Axis Magnetic Anisotropy and Determination of Anisotropic Parameters of LnIII−CuII Single-Molecule Magnets. *Chem. - Eur. J*. **2011**, *17*, 196−205. (c) Watanabe, A.; Yamashita, A.; Nakano, M.; Yamamura, T.; Kajiwara, T. Multi-Path Magnetic Relaxation of Mono-Dysprosium(III) Single-Molecule Magnet with Extremely High Barrier. *Chem. - Eur. J*. **2011**, *17*, 7428−7432.

28.-Abragam, A.; Bleaney, B. *Electron Paramagnetic Resonance of Transition Ions*, Clarendon Press. Oxford, **1970**.

29.-Marx, R.; Moro, F.; Dörfel, M.; Ungur, L.; Waters, M.; Jiang, S. D.; Orlita, M.; Taylor, J.; Frey, W.; van Slageren J. Spectroscopic determination of crystal field splittings in lanthanide double deckers. *Chem. Sci.* **2014**, *5*, 3287-3293.

30.- Gómez-Coca, S.; Aravena, D.; Morales, R.; Ruiz, E. Large magnetic anisotropy in mononuclear metal complexes.*Coord. Chem. Rev.*, **2015**, *289*, 379-392.

31.-Ungur, L.; Thewissen, M.; Costes, J. P.; Wernsdorfer, W.; Chibotaru, L. F. Interplay of strongly anisotropic metal ions in magnetic blocking of complexes. *Inorg.Chem.* **2013**, *52*, 6328−6337.

32.- a) Venugopal, A.; Tuna, F.; Spaniol, T. P.; Ungur, L.; Chibotaru, L. F.; Okuda, J.; Layfield, R. A. A hydride-ligated dysprosium single-molecule magnet. *Chem. Commun*. **2013**, *49*, 901-903.b) Habib, F.; Brunet, G.; Vieru, V.; Korobkov, I.; Chibotaru, L. F.; Murugesu, M. Significant Enhancement of Energy Barriers in Dinuclear Dysprosium Single-Molecule Magnets Through Electron-Withdrawing Effects. *J. Am. Chem. Soc.*, **2013**, *135*,13242–13245. c) Zhang, K.; Yuan, C.; Guo, F-S.; Zhang, Y-Q.; Wang, Y-Y. Fine-tuning terminal solvent ligands to rationally enhance the energy barrier in dinuclear dysprosium single-molecule magnets, *Dalton Trans.*, **2017**,*46*, 186-192. d) Tuna, F.; Smith, C. A.; Bodensteiner, M.;Ungur, L.;Chibotaru, L. F.; McInnes, E. J. L.;Winpenny, R. E. P.; Collison, D.; Layfield, R. A. A High Anisotropy Barrier in a Sulfur-Bridged Organodysprosium Single-Molecule Magnet. *Angew. Chem. Int. Ed.*,**2012**, *51*, 6976–6980. e) Guo, Y-N.; Xu, G-F.; Wernsdorfer, W.; Ungur, L.; Guo, Y.; Tang, J.; Zhang, H-J.; Chibotaru, L. F.; Powell, A. K. Strong Axiality and Ising Exchange Interaction Suppress Zero-Field Tunneling of Magnetization of an Asymmetric Dy2 Single-Molecule Magnet. *J. Am. Chem. Soc.*, **2011**,*133*, 11948-11951.

33.- Upadhyay, A.; Singh, S. K.; Das, C.; Mondol, R.; Langley, S. K.; Murray, K. S.; Rajaraman, G.; Shanmugam, M. Enhancing the effective energy barrier of a Dy(III) SMM using a bridged diamagnetic Zn(II) ion. *Chem. Commun.*,**2014**, *50*, 8838– 8841.

34.- Liu, J.-L.; Chen, Y.-C.; Zheng, Y.-Z.; Lin, W.-Q.; Ungur, L.; Wernsdorfer, W.; Chibotaru, L. F.; Tong, M.-L. Switching the anisotropy barrier of a single-ion magnet by symmetry change from quasi-D_{5h} to quasi-O_h.*Chem. Sci*. **2013**, *4*, 3310–3316.

35.- Oyarzabal, I.; Rodríguez-Diéguez, A.; Barquín, M.; Seco, J. M.; Colacio, E. The effect of the disposition of coordinated oxygen atoms on the magnitude of the energy barrier for magnetization reversal in a family of linear trinuclear Zn–Dy–Zn complexes with a square-antiprism DyO_8 coordination sphere, *Dalton Trans.*, **2017**, *46*, 4278–4286.

36.-Saito, K.; Miyashita, S. Magnetic Foehn Effect in Adiabatic Transition. *J. Phys. Soc. Japan***2001**, *70*, 3385 – 3390.